mathematics

Article

Diverse Forms of Breathers and Rogue Wave Solutions for the Complex Cubic Quintic Ginzburg Landau Equation with Intrapulse Raman Scattering

Aly R. Seadawy [1,*], Hanadi Zahed [1] and Syed T. R. Rizvi [2]

[1] Mathematics Department, Faculty of Science, Taibah University, Al-Madinah Al-Munawarah 41411, Saudi Arabia; hzahed@taibahu.edu.sa

[2] Department of Mathematics, COMSATS University Islamabad, Lahore Campus, Lahore 54000, Pakistan; strrizvi@gmail.com

* Correspondence: aabdelalim@taibahu.edu.sa

Abstract: This manuscript consist of diverse forms of lump: lump one stripe, lump two stripe, generalized breathers, Akhmediev breather, multiwave, M-shaped rational and rogue wave solutions for the complex cubic quintic Ginzburg Landau (CQGL) equation with intrapulse Raman scattering (IRS) via appropriate transformations approach. Furthermore, it includes homoclinic, Ma and Kuznetsov-Ma breather and their relating rogue waves and some interactional solutions, including an interactional approach with the help of the double exponential function. We have elaborated the kink cross-rational (KCR) solutions and periodic cross-rational (KCR) solutions with their graphical slots. We have also constituted some of our solutions in distinct dimensions by means of 3D and contours profiles to anticipate the wave propagation. Parameter domains are delineated in which these exact localized soliton solutions exit in the proposed model.

Keywords: NLSE; lump solitons; breathers; multiwave

MSC: 35J05; 35J10; 35K05; 35L05

Citation: Seadawy, A.R.; Zahed, H.; Rizvi, S.T.R. Diverse Forms of Breathers and Rogue Wave Solutions for the Complex Cubic Quintic Ginzburg Landau Equation with Intrapulse Raman Scattering. *Mathematics* **2022**, *10*, 1818. https://doi.org/10.3390/math10111818

Academic Editor: Nikolai A. Kudryashov

Received: 25 March 2022
Accepted: 18 May 2022
Published: 25 May 2022

1. Introduction

The analysis of the solitary wave solutions (SWs) for various nonlinear partial differential Equations (NLPDEs) play a significant role in different aspects of mathematical and physical phenomena [1–5]. Mainly natural phenomena arising in applied science, such as nuclear physics, chemical reactions, optical fibres [6–10], fluid mechanics, plasma, physics and ecology, can sometimes be modeled and described by NLPDEs [11–21]. Constructing the SWs of these equations has become a global interest in recent years. Hence, an enormous number of mathematical experts have attempted to invent various approaches by which one can obtain the exact solutions of such equations. Nowadays, some new effective techniques have been residential and well known [22]. To learn the mechanism of phenomena for the NLPDEs in physics and engineering, their SWs are calculated. There are many integration architectonics, such as Lie symmetry analysis [23], Backlund transformations [24], conservation laws, symmetry bifurcation [25], extended tanh-function, spontaneous symmetry [26], Painleve and Lie symmetries [27], CESTAC Method [28], polynomial law [29], computational architectonic, Semi inverse technique [30], HBM [31], mapping algorithm [32], (G'/G) expansion algorithm [33], Kudryashove architectonic [34], auxiliary equation scheme [35] and $\exp((-\varphi'/\varphi)\eta)$-expansion scheme [36]. The Riccati-Bernoulli sub-ODE method, optimal homotopy asymptotic approach, Exp-function algorithm, sine-cosine process, tanh-sech mechanism, extended tanh-scheme, F-expansion method, homogeneous balance technique, Jacobi elliptic function mechanism and several others have been developed to obtain SWs. A massive number of NLPDEs can be purely solved by the abovementioned methods. However, there is no a specific approach by which we can deal with all NLPDEs. In addition, some NLPDEs cannot be effortlessly solved by most traditional methods. The proposed method, which allows us to execute tedious and sophisticated algebraic calculations, is utilized to establish solitary wave solutions, peaked wave solutions and exact wave solutions for NLPDEs.

The NLPDEs are mainly valuable zones for nonlinear optics to reveal the proliferation distinctively short pulse in ultra-fast signal routing and telecommunication and light pulse propagation in condensed matter [37–41]. There are lots of recognized model, such as the modified KP-Equation [24], Fokas Equation [23], rth Dym Equation [21], Pochhammer-Chree model [14], modified Equation [11], fractional NLSE [20], fiber Bragg gratings model [29], Einstein's vacuum field Equation [27], double-chain model [13], Wazwaz Benjamin model [12], modified Veronese Web Equation [42], (KMN)-Equation [30], Sawada Kotera Equation [31] and Fokas–Lenells model.

Recently, lump and interactional solutions (LISs) have shown significance to depict the wave features for various NLPDEs. For instance, LISs were studied by Zhou et al. with the Hirota Satsuma model [43], LIsS were found by Wang et al. with the Burgers model [44], Wu et al. worked on lump, periodic lump solutions in the KP model [45] and, similarly, Li et al. studied various lumps for BLMP model [46]. Breather soliton is a nonlinear wave in which energy is localized in space but oscillates in time, or vice versa, and has been newly reported in an optical fiber cavity. Cavity solitons (CSs) are localized pulses of light that can be wound up in nonlinear optical resonators and have sparked imperative study curiosity in the perspective of micro resonator-based frequency comb generation, and are found in a range of subfields of natural science, for instance fluid dynamics, solid-state physics, plasma physics, molecular biology, chemistry and nonlinear optics [47]. Recently, Rizvi et al. investigated breathers for NLEE [15], Seadawy et al. interpreted breather solutions for NLEE [42], Ahmed et al. studied breathers for the general $(2+1)$-rth dispersionless Equation [21], and Ahmed et al. found kinky breathers for the nonlinear model [48], among many other studies. Multiwave solutions (MS) for nonlinear models have its own worth. Seadawy et al. worked on MS for the HS-Equation [15], Ahmed et al. studied MS for the $(2+1)$-rth dispersionless Equation [21], Rizvi et al. reported MS for NLEE [42], Seadawy et al. worked on MS for the nonlinear model [48], Wazwaz analyzed rogue wave and breathers [49], etc.

In this template, we begin our analysis by taking the CQGL-equation with IRS term [22];

$$i\Delta_z + \frac{1}{2}\Delta_{tt} + \gamma|\Delta|^2\Delta = i\delta\Delta + i\beta\Delta_{tt} + i\varepsilon|\Delta|^2\Delta - \nu|\Delta|^4\Delta + i\mu|\Delta|^4\Delta + T_r\left(|\Delta|^2\right)_t\Delta, \tag{1}$$

where z is the normalized propagation distance, t is the retarded time and Δ is the normalized envelope of the pulse. For a laser system, the interpretation of distinct coefficients is as follows: β shows spectral filtering or gain dispersion, μ expresses higher-order correction to the nonlinear absorption or amplification, ϵ shows nonlinear gain, ν shows a higher-order correction term to the nonlinear refractive index, T_r shows the IRS coefficient, γ displays the positive Kerr effect (or negative Kerr effect if negative) and δ is a constant gain (or loss if negative). The stated equation is a canonical model for weakly nonlinear, dissipative systems and one of the most studied nonlinear equations in the physics community. It can be used to describe a vast variety of nonlinear phenomena, such as Bose–Einstein condensation, superconductivity, strings in field theory, superfluidity, lasers and liquid crystals.

In order to solve Equation (1), we insert $\Delta = p + iq$, where $|\Delta| = \sqrt{p^2+q^2}$. Thus, Equation (1) may be converted into real and imaginary parts:

$$\begin{cases} p^3\gamma + q^2\gamma p + p^5\nu + 2p^3q^2\nu + q^4\nu p + \delta q + p^2\varepsilon q + q^3\varepsilon + p^4\mu q + 2p^2q^3\mu + q^5\mu + \frac{1}{2}p_{tt} + \beta q_{tt} - q_z = 0, \\ -\delta p - p^3\varepsilon - q^2\varepsilon p - \mu p^5 - 2\mu p^3q^2 - \mu q^4 p + \gamma p^2 q + \gamma q^3 + \nu p^4 q + 2\nu p^2q^3 + \nu q^5 - \beta p_{tt} + \frac{1}{2}q_{tt} + p_z = 0. \end{cases} \tag{2}$$

The document for the upcoming sections will be detailed in a sequence: in Section 2, we will evaluate the lump solutions for the proposed model form with few graphical slots. In Section 3, there will be a concise discussion of lump one stripe solutions with some 3D and contour graphical slots. In Section 4, we will construct lump two stripe results with some suitable profiles. Section 5 consist of a Ma-breather (MB) and its relating rogue wave. Similarly, in Section 6, we will evaluate the Kuznetsov-Ma breather (KMB) with some suitable 3D and contour shapes. In Section 7, we will find the generalized breathers (GB) for proposed equation with their relating figures. Section 8 includes Akhmediev breathers (AB) along with some profiles for the concerned model. Similarly, Section 9 will detail the procedure to construct standard rogue waves. In Section 10, we will explain the methodology for finding multiwave solutions. In the same way, we will compute homoclinic breathers for the proposed equation in Section 11. There will be M-shaped solitons in Section 12. In Section 13, there will be an interaction approach for the proposed model. We will find kink cross-rational (KCR) solutions in Section 14. Section 15 includes periodic cross-rational (PCR) solutions along with some 3D and contour profiles for the concerned model. Section 16 contains the results and a discussion about our newly achieved solutions and we will make an suitable comparison with earlier work. Finally, in Section 17, we will provide some concluding annotations.

2. Lump Solution

For the lump solutions of Equation (2), we apply the subsequent ansatz [43,44]:

$$p = \frac{6}{\rho}(\ln g)_z\,, \quad q = \frac{6}{\omega}(\ln h)_z\,, \tag{3}$$

and get the proceeding form:

$$\begin{aligned}&2p^2\gamma\omega g^2h^3g_z + 2q^2\gamma\omega g^2h^3g_z + 2p^4\nu\omega g^2h^3g_z + 4p^2q^2\gamma\omega g^2h^3g_z + 2q^4\nu\omega g^2h^3g_z\\ &+2\omega h^3g_t^2g_z - \omega gh^3g_{tt}g_z + 2\delta\rho g^3h^2h_z + 2p^2\varepsilon\rho g^3h^2h_z + 2q^2\varepsilon\rho g^3h^2h_z + 2p^4\mu\rho g^3h^2h_z\\ &+4p^2q^2\mu\rho g^3h^2h_z + 2q^4\mu\rho g^3h^2h_z + 4\beta\rho g^3h_t^2h_z + \ldots + 2\beta\rho g^3h^2h_{ztt} - 2\rho g^3h^2h_{zz} = 0.\end{aligned} \tag{4}$$

Now, the function g and h in Equation (4) can be considered as [43,44]:

$$g = \xi_1^2 + \xi_2^2 + a_2, \quad h = \xi_1^2 + \xi_2^2 + a_3, \tag{5}$$

where $\xi_1 = a_0z + t$, $\xi_2 = a_1z + t$., while $a_i(1 \leq i \leq 3)$ are specific real parameters. Now, using g and h into Equation (4) and solving the coefficients of the z and t implies:

Set I. When

$$a_0 = \left(-4+\sqrt{15}\right)a_1, a_1 = a_1, a_2 = 0, \rho = \rho, \omega = \omega. \tag{6}$$

These generated parameters make the lump solution:

$$\Delta_1 = \frac{-6\left(-4+\sqrt{15}\right)R_1 + \left(-4+\sqrt{15}\right)^2a_1^2\left(2a_1(t+a_1z) + 2\left(-4+\sqrt{15}\right)a_1R_2\right)}{a_1^2\left((t+a_1z)^2 + \left(t+\left(-4+\sqrt{15}\right)a_1z\right)^2\right)} + \Omega_1, \tag{7}$$

where $R_1 = a_1^2 + \left(-4+\sqrt{15}\right)a_1^2, \Omega_1 = \dfrac{6i\left(2a_1(t+a_1z)+2\left(-4+\sqrt{15}\right)a_1\left(t+\left(-4+\sqrt{15}\right)a_1z\right)\right)}{\left(\frac{\left(-4+\sqrt{15}\right)^2a_1^3}{a_1^3-\left(-4+\sqrt{15}\right)a_1^3+\left(-4+\sqrt{15}\right)a_1^3}+(t+a_1x)^2+\left(t+\left(-4+\sqrt{15}\right)a_1z\right)^2\right)\omega}$
and $R_2 = t + \left(-4+\sqrt{15}\right)a_1z.$

3. Lump One Stripe Solution

To get the lump one stripe solution, we apply the transformation shown in Equation (4) [50]:

$$g = \xi_1^2 + \xi_2^2 + a_2 + b_0 e^{k_1 z + k_2 t}\ , \quad h = \xi_1^2 + \xi_2^2 + a_3 + b_0 e^{k_1 z + k_2 t}, \tag{8}$$

where $\xi_1 = a_0 z + t$, $\xi_2 = a_1 z + t$., while $a_i (1 \le i \le 3)$, k_1, k_2 and b_0 are any specific real parameters. Now, using g and h in Equation (4) and solving the coefficients of the z and t:

Set I. When $a_2 = 0$:

$$a_0 = -a_1, a_3 = \frac{-6b_0\omega}{b_0\omega(\nu p^6 q^2 + \nu q^4 + \gamma p^2 + \gamma q^2)}, a_5 = a_5, \omega = \omega, \rho = \rho, k_2 = 0. \tag{9}$$

These parameters exhibit the required solution to Equation (2):

$$\Delta_2 = \frac{6\Big(b_0 e^{k_1 z} k_1 - 2a_1(t - a_1 z) + 2a_1(t + a_1 z)\Big)}{\rho\Big(b_0 e^{k_1 z} + (t - a_1 z)^2 + (t + a_1 z)^2\Big)} + \Omega_2. \tag{10}$$

where $\Omega_2 = \frac{6i\left(b_0 e^{k_1 z} k_1 - 2a_1(t - a_1 z) + 2a_1(t + a_1 z)\right)}{\left(b_0 e^{k_1 z} + (t - a_1 z)^2 + (t + a_1 z)^2 - \frac{6}{p^2\gamma + q^2\gamma + p^4\nu + 2p^2q^2\nu + q^4\nu}\right)\omega}$.

4. Lump Two Stripe Solution

To obtain the lump two stripe solution, we assume the subsequent transformation in Equation (4) [50]:

$$g = \xi_1^2 + \xi_2^2 + a_2 + b_0 e^{k_1 z + k_2 t} + b_1 e^{k_3 z + k_4 t}\ , \quad h = \xi_1^2 + \xi_2^2 + a_3 + b_0 e^{k_1 z + k_2 t} + b_1 e^{k_3 z + k_4 t}, \tag{11}$$

where $\xi_1 = a_0 z + t$, $\xi_2 = a_1 z + t$., while $a_i(1 \le i \le 3)$, k_1, k_2, k_3, k_4, b_0 and b_1 are any specific real parameters. Now, using g and h in Equation (4) and solving the coefficients of the z and t:

Set I. When $a_1 = a_2 = a_3 = 0$:

$$a_0 = a_0, a_5 = a_5, b_1 = \frac{-5k_3\delta}{7k_3^2 - 5k_3\delta}, \beta = \frac{b_1\omega\left(7k_3{}^2 - 5k_3\delta\right)}{10b_1k_3\delta\rho}, \rho = \frac{-4k_3^2 + 5k_3}{5k_3}. \tag{12}$$

These parameters exhibits the required solution to Equation (2):

$$\Delta_3 = \frac{6\left(b_0 e^{k_2 t + k_1 z} k_1 - \frac{e^{k_4 t + k_3 z} k_3 (5k_3 - 4k_3^2)}{-5k_3 + 11k_3^2} + R_3\right)}{\rho\left(b_0 e^{k_2 t + k_1 z} k_1 - \frac{e^{k_4 t + k_3 z} k_3 (5k_3 - 4k_3^2)}{-5k_3 + 11k_3^2} + R_4\right)} + \frac{6i\left(b_0 e^{k_2 t + k_1 z} k_1 - \frac{e^{k_4 t + k_3 z} k_3 (5k_3 - 4k_3^2)}{-5k_3 + 11k_3^2} + R_3\right)}{\omega\left(b_0 e^{k_2 t + k_1 z} k_1 - \frac{e^{k_4 t + k_3 z} k_3 (5k_3 - 4k_3^2)}{-5k_3 + 11k_3^2} + R_4\right)}, \tag{13}$$

where $R_3 = 2a_0(t + a_0 z)$ and $R_4 = t^2 + (t + a_0 z)^2$.

5. Ma-Breather (MB) and Its Relating Rogue Wave

We assume g and h in Equation (4) as [44]:

$$g = 1 + \alpha_1 + e^{i(p_1 x)} + e^{-i(p_1 x)} e^{\lambda_1 t + \gamma_1} + \beta_1 e^{2(\lambda_1 t + \gamma_1)}\ , \quad h = 1 + \alpha_2 + e^{i(p_2 x)} + e^{-i(p_2 x)} e^{\lambda_2 t + \gamma_2} + \beta_2 e^{2(\lambda_2 t + \gamma_2)}, \tag{14}$$

where α_1, α_2, p_1, p_2, λ_1, λ_2, γ_1 and γ_2 are any parameters. Now, using g and h in Equation (4) and letting the coefficients of exp and cos functions be zero:

Set I. When $\gamma_1 = \beta_2 = 0$:

$$\alpha_1 = \alpha_1, \alpha_2 = \alpha_2, \mu = \frac{ip_2 - 2\delta - 2p^2\varepsilon - 2q^2\varepsilon - 5\beta\lambda_2^2}{2(p^2 + q^2)^2}, p_1 = p_1, a_4 = a_4. \tag{15}$$

These parameters form the Ma-breather solution to Equation (1):

$$\Delta_4 = \frac{6e^{t\lambda_1}\left(-ie^{-ip_1z}p_1 + ie^{ip_1z}p_1\right)\alpha_1}{\left(1+e^{t\lambda_1}\left(e^{-ip_1z}+e^{ip_1z}\right)\alpha_1\right)\rho} + \frac{6ie^{\gamma_2+t\lambda_2}\left(-ie^{-ip_2z}p_2 + ie^{ip_2z}p_2\right)\alpha_2}{\left(1+e^{\gamma_2+t\lambda_2}\left(e^{-ip_2z}+e^{ip_2z}\right)\alpha_2 + e^{2(\gamma_2+t\lambda_2)}\beta_2\right)\omega}. \tag{16}$$

6. Kuznetsov-Ma Breather (KMB) and Its Relating Rogue Wave

We assume g and h in Equation (4) as [44]:

$$\begin{aligned} g &= e^{-p_1(b_2z-b_1t)} + a_1\cos(p(b_2z+b_1t)) + a_2\cos(p(b_2z-b_1t)), \\ h &= e^{-p_2(b_3z-b_4t)} + a_3\cos(p(b_3z+b_4t)) + a_4\cos(p(b_3z-b_4t)), \end{aligned} \tag{17}$$

where p_1, p_2, b_1, b_2, b_3, b_4, a_1, a_2, a_3 and a_4 are any parameters to be found. Now, using g and h in Equation (4) and letting the coefficients of exp and cos functions be zero follows:

Set I. When:

$$p_1 = p_1, \nu = \frac{-p_1^2(\gamma^2+\mu)}{p^2}, a_1 = a_1, \gamma = \gamma, a_3 = a_3, \rho = \rho. \tag{18}$$

These parameters form the proposed solution to Equation (1):

$$\Delta_5 = \frac{6\Big(-b_2e^{-p_1(-b_1t+b_2z)}p_1 + a_2b_2e^{p_1(-b_1t+b_2z)}p_1 - a_1b_2p\sin(p(b_1t+b_2z))\Big)}{\rho\left(e^{-p_1(-b_1t+b_2z)} + a_2e^{p_1(-b_1t+b_2z)} + a_1\cos(p(b_1t+b_2z))\right)} + \Omega_3, \tag{19}$$

where $\Omega_3 = \dfrac{6i\Big(-b_3e^{-p_2(-b_3t+b_4z)}p_2 + a_4b_3e^{-p_2(-b_3t+b_4z)}p_2 - a_3b_3p\sin(p(b_4t+b_3z))\Big)}{\omega\Big(e^{-p_2(-b_3t+b_4z)} + a_4e^{p_2(-b_3t+b_4z)} + a_3\cos(p(b_4t+b_3z))\Big)}$.

7. Generalized Breathers (GB)

In order to obtain generalized breathers we use ansatz [51]:

$$\Delta(z,t) = 2bc\left(\frac{6}{\kappa}\ln\Psi(z,t)\right)_z + m, \tag{20}$$

where b, c and m are any particular constants. Inserting Equation (20) into Equation (1), we have:

$$\begin{aligned} &m^3\gamma\kappa^5\psi^5 - im\delta\kappa^5\psi^5 - im^3\varepsilon\kappa^5\psi^5 + m^5\kappa^5\nu\psi^5 + m^5\kappa^5\nu\psi^5 + 36bcm^2\gamma\kappa^4\psi^4\psi_z - 12ibc\delta\kappa^4\psi^4\psi_z \\ &-36ibcm^2\varepsilon\kappa^4\psi^4\psi_z - 60ibcm^4\mu\kappa^4\psi^4\psi_z + 60bcm^4\nu\kappa^4\psi^4\psi_z + 12bcmT_r\kappa^4\psi^3\psi_t\psi_z + 12bc\kappa^4\psi^2\psi_z\psi_t^2 \\ &-24ibc\beta\kappa^4\psi^2\psi_t^2\psi_z - 6bc\kappa^4\psi^3\psi_{tt}\psi_z + 12ibc\beta\kappa^4\psi^3\psi_{tt}\psi_z + \ldots + 12ibc\kappa^4\psi^4\psi_{zz} - 12ibc\beta\kappa^4\psi^4\psi_{zt} = 0. \end{aligned} \tag{21}$$

For finding the required solutions, we use the following assumption in Equation (21):

$$\psi = \frac{(1-4c)\cosh(\sigma t) + \sqrt{2c}\cos(\rho z) + i\sigma\sinh(\sigma t)}{\sqrt{2c}\cos(\rho z) - \cosh(\sigma t)}e^{it}, \tag{22}$$

where σ, ρ and c are constants to be found. The coefficients of cosh, sinh and exp functions are defined as follows:

$$a = a, b = b, m = 0, c = \frac{1}{2}, \rho = \rho, \sigma = \sigma. \tag{23}$$

These values implies the following GB profiles of Equation (1):

$$\Delta_6 = \frac{6bie^{-it}(\cos(\rho z) - \cosh(\sigma t))\left(\frac{-e^{it}\rho\sin((\rho z))}{\cos(\rho z)-\cosh(\sigma t)} + \frac{e^{it}\rho\sin((\rho z))(\cos((\rho z))-\cosh(\sigma t)+i\sigma\sinh(\sigma t))}{(\cos(\rho z)-\cosh(\sigma t))^2}\right)}{\kappa\cos(\rho z) - \cosh(\sigma t) + i\sigma\sinh(\sigma t)}. \tag{24}$$

8. Akhmediev Breathers (AB)

We use the following transformation in Equation (21) [52]:

$$\psi = \sqrt{p_0}\frac{(1-4a)\cosh(bz) + ib\sinh(bz) + \sqrt{2a}\cos(\omega_{\text{ mod }}T)}{\sqrt{2a}\cos(\omega_{\text{ mod }}T) - \cosh(b\xi)}, \tag{25}$$

where ω_{mod} interprets the perturbation frequency (PF) with p_0 as the power. The coefficients a and b depends on ω_{mod} and are defined by $2a = 1 - (\frac{\omega_{mod}}{\omega_c})^2$ and $b = [8a(1-2a)]^2$ with $\omega_c^2 = \frac{4p_0\gamma}{|\beta_2|}$. Setting the coefficients of trigonometric and hyperbolic functions be zero:

$$a = a, b = b, c = c, \omega = \sqrt{\frac{4-82}{2i\beta}}, \rho = \rho, p_0 = p_0. \tag{26}$$

These values imply the AB of Equation (1) to be as follows:

$$\Delta_7 = m + \frac{12bc\left(\sqrt{2a}\cos\left(\frac{t\sqrt{-\frac{i(4-8a)}{\beta}}}{\sqrt{2}}\right) - \cosh(bz)\right)\Omega_4}{\sqrt{p_0}\kappa\left(\sqrt{2a}\cos\left(\frac{t\sqrt{-\frac{i(4-8a)}{\beta}}}{\sqrt{2}}\right) + (1-4a)\cosh(bz) + ib\sinh(bz)\right)}, \tag{27}$$

where:

$$\Omega_4 = \left(\frac{b\sqrt{p_0}\sinh(bz)\left(\sqrt{2a}\cos\left(\frac{t\sqrt{-\frac{i(4-8a)}{\beta}}}{\sqrt{2}}\right) + (1-4a)\cosh(bz) + ib\sinh(bz)\right)}{\left(\sqrt{2a}\cos\left(\frac{t\sqrt{-\frac{i(4-8a)}{\beta}}}{\sqrt{2}}\right) - \cosh(bz)\right)^2} + \frac{\sqrt{p_0}\left(ib^2\cosh(bz) + (1-4a)b\sinh(bz)\right)}{\sqrt{2a}\cos\left(\frac{t\sqrt{-\frac{i(4-8a)}{\beta}}}{\sqrt{2}}\right) - \cosh(bz)}\right).$$

9. Standard Rogue Wave (SRW) Solutions

For evaluating the SRW, we apply the subsequent assumption in Equation (21) [44]:

$$\psi = -\left(1 - \frac{4(1+2it)}{1+4z^2+4t^2}\right)e^{it}, \tag{28}$$

Setting the coefficients of exponential function, z and t be zero will follow:

$$b = b, \beta = \frac{-i}{2}, m = \sqrt{\frac{-3i\varepsilon + 3\gamma + \sqrt{20\delta\mu - 9\varepsilon^2 - 18i\gamma\varepsilon + 20i\delta\nu + 9\gamma^2}}{10(i\mu - \nu)}}, c = c, \kappa = \kappa. \tag{29}$$

These values implies the SRW to Equation (1):

$$\Delta_8 = -\frac{384bc(1+2it)z}{(1+4t^2+4z^2)\left(-1+\frac{4(1+2it)}{1+4t^2+4z^2}\right)\kappa} + \sqrt{\frac{-3i\varepsilon + 3\gamma + \sqrt{20\delta\mu - 9\varepsilon^2 - 18i\gamma\varepsilon + 20i\delta\nu + 9\gamma^2}}{10(i\mu - \nu)}}. \tag{30}$$

10. Multiwaves Solutions (MS)

For these type of results, we use the preceding transformation in Equation (2) [48]:

$$\Delta(z,t) = \psi(\xi)e^{\iota\theta}, \;\; \xi = k_1 z - c_1 t, \;\; \theta = k_2 z - c_2 t. \tag{31}$$

Using the above transformation, we obtain the real and imaginary parts of equal Equation (2), by considering the real part only:

$$\gamma\psi^3 + \nu\psi^5 + c_1 T_r\psi\psi' - \frac{1}{2}c_1^2\psi + \frac{1}{2}c_1^2\psi'' + 2\beta c_1 c_2\psi' = 0. \tag{32}$$

Now, by way of following the assumption in Equation (32):

$$\psi = 2(\ln f)_{\xi}, \tag{33}$$

we obtain:

$$-c_2^2 f^4 f' - 4\beta c_1 c_2 f^3 f'^2 + 2c_1^2 f^2 f'^3 + 8\gamma f^2 f'^3 - 4c_1 T_r f^2 f'^3 + 32\nu f'^5 + 4c_1 c_2 \beta f^4 f'' - 3c_1^2 f^3 f' f'' \\ +4c_1 f^3 T_r f' f'' + c_1^2 f^4 f''' = 0 \tag{34}$$

To get the MS of Equation (34), we use anstaz [48]:

$$f = b_0 \cosh(a_1\xi + a_2) + b_1 \cos(a_3\xi + a_4) + b_2 \cosh(a_5\xi + a_6), \tag{35}$$

where a_1, a_2, a_3, a_4, a_5 and a_6 are any specific constants. Substituting Equation (35) into Equation (34) with Mathematica and letting the coefficients of hyperbolic and trigonometric functions to zero:

Set I. When:

$$a_1 = a_1, a_2 = a_2, a_3 = \frac{-1}{2}a_5, a_4 = a_4, a_5 = a_5, b_0 = 0, b_1 = b_1, c_1 = c_1. \tag{36}$$

Using the above values, we have:

$$\Delta_9 = \frac{2e^{i(-c_2t+k_2z)}\left(\frac{1}{2}a_5 b_1 \cos\left(a_4 - \frac{1}{2}a_5(-c_1t + k_1z)\right)\sin\left(a_4 - \frac{1}{2}a_5(-c_1t + k_1z)\right) + \Omega_5\right)}{b_1 \cos\left(a_4 - \frac{1}{2}a_5(-c_1t + k_1z)\right) + b_2 \cosh(a_6 + a_5(-c_1t + k_1z))}, \tag{37}$$

where $\Omega_5 = a_5 b_2 \cosh(a_6 + a_5(-c_1t + k_1z)) \sinh(a_6 + a_5(-c_1t + k_1z))$.

11. Homoclinic Breather (HB)

In this approach we assume f the form [48]:

$$f = e^{-p(a_2+a_1\xi)} + b_1 e^{p(a_4+a_3\xi)} + b_0 \cos(p_1(a_6 + a_5\xi)), \tag{38}$$

where $a_i's$ denotes any particular constants. Inserting Equation (38) into Equation (34) and collecting coefficients of exponential and trigonometric functions to be zero yields:

Set I. When:

$$a_1 = \frac{1}{2}a_5, a_2 = a_2, a_3 = a_3, c_1 = \frac{-2a_5^2 \nu p^2}{T_r}, b_1 = b_1, a_5 = a_5. \tag{39}$$

Via the above values we obtain:

$$\Delta_{10} = \frac{2\left(\frac{-1}{2}a_5 b_1 p e^{p\left(a_4 - \frac{1}{2}a_4\left(k_1z + \frac{2a_5^2p^2t\nu}{T_r}\right)\right)} - \frac{1}{2}a_5 p e^{-p\left(a_2 - \frac{1}{2}a_5\left(k_1z + \frac{2a_5^2p^2t\nu}{T_r}\right)\right)}\right)e^{i(-c_2t+k_2z)}}{b_1 e^{p\left(a_4 - \frac{1}{2}a_4\left(k_1z + \frac{2a_5^2p^2t\nu}{T_r}\right)\right)} + e^{-p\left(a_2 - \frac{1}{2}a_5\left(k_1z + \frac{2a_5^2p^2t\nu}{T_r}\right)\right)}}. \tag{40}$$

12. *M*-Shaped Rational Solitons

For these solutions, we consider the form [48,53]:

$$f = (d_1\xi + d_2)^2 + (d_3\xi + d_4)^2 + d_5, \tag{41}$$

where $d_i (1 \leq i \leq 5)$, are any parameters. Put f into Equation (34) and solving coefficients of ξ to get subsequent result on parameters:

Set I. Whenever $d_5 = d_2 = 0$:

$$d_1 = id_3, d_3 = d_3, d_4 = \frac{c_1^2 d_3 \sqrt{c_1^4 d_3^2} + 24\beta c_1 c_2 \gamma}{6\beta c_1 c_2}, c_1 = c_1, c_2 = c_2. \tag{42}$$

Using the above values, we obtain:

$$\Delta_{11} = \frac{2e^{i(-c_2 t + k_2 z)}\left(-2d_3^2(-c_1 t + k_1 z) + 2d_3\left(d_3(-c_1 t + k_1 z) + \frac{c_1^2 d_3 \sqrt{c_1^4 d_3^2 + 24\beta c_1 c_2 \gamma}}{6\beta c_1 c_2}\right)\right)}{-{d_3}^2(-c_1 t + k_1 z)^2 + \left(d_3(-c_1 t + k_1 z) + \frac{c_1^2 d_3 \sqrt{c_1^4 d_3^2 + 24\beta c_1 c_2 \gamma}}{6\beta c_1 c_2}\right)^2}. \tag{43}$$

13. Interactional Solutions with Double Exponential Form

We use the following hypothesis [48]:

$$f = b_1 e^{-a_1 \xi + a_2} + b_2 e^{a_3 \xi + a_4}. \tag{44}$$

where a_1, a_2, a_3 and a_4 are some constants. Inserting Equation (44) into Equation (34) and solving coefficients of exponential functions, a system of equations is obtained. By solving it:

Set I.

$$a_1 = \left(2 - \sqrt{3}\right)a_3, a_2 = a_2, c_1 = \frac{8a_3^2 \nu\left(7 - 4\sqrt{3}\right)}{T_r}, a_3 = a_3, a_4 = a_4. \tag{45}$$

Using the above values we have:

$$\Delta_{12} = \frac{2\left(a_3 b_2 e^{a_4 + a_3\left(k_1 z - \frac{8(7-4\sqrt{3})a_3^2 t\nu}{T_r}\right)} + \left(2 - \sqrt{3}\right)a_3 b_1 e^{a_2 + (2-\sqrt{3})a_3\left(k_1 z - \frac{8(7-4\sqrt{3})a_3^2 t\nu}{T_r}\right)}\right)e^{i(-c_2 t + k_2 z)}}{b_2 e^{a_4 + a_3\left(k_1 z - \frac{8(7-4\sqrt{3})a_3^2 t\nu}{T_r}\right)} + b_1 e^{a_2 + (2-\sqrt{3})a_3\left(k_1 z - \frac{8(7-4\sqrt{3})a_3^2 t\nu}{T_r}\right)}}. \tag{46}$$

14. Kink Cross-Rational (KCR) Solutions

For KCR solutions, we consider f as [54,55]:

$$f = g_0 + e^{-(a_1\xi + a_2)} + k_1 e^{a_1 \xi + a_2} + (b_1 \xi + b_2)^2 + (b_3 \xi + b_4)^2, \tag{47}$$

where a_i and b_i are some constants. Inserting Equation (47) into Equation (34) and solving coefficients of exponential functions:

Set I.

$$a_1 = \sqrt{\frac{-3}{32\mu}}c_1, b_1 = b_1, b_2 = b_2, k_1 = 0, a_2 = a_2, \nu = \frac{2}{5}\mu, T_r = \frac{3\sqrt{\frac{-3}{32\mu}}c_1^2 + 8\beta c_2}{4\sqrt{\frac{-3}{32\mu}}c_1}, b_3 = b_3, b_4 = b_4. \tag{48}$$

Using the above values we have:

$$\Delta_{13} = \frac{2e^{i(-c_2 t + k_2 z)}\left(-2b_1(b_2 - b_1 c_2 t) + 2b_3(b_4 - b_3 c_2 t) - \frac{1}{4}\sqrt{-\frac{3}{2\mu}}c_2 e^{-a_2 + \frac{1}{4}\sqrt{-\frac{3}{2\mu}}c_2^2 t}\right)}{e^{-a_2 + \frac{1}{4}\sqrt{-\frac{3}{2\mu}}c_2^2 t} + g_0 + (b_2 - b_1 c_2 t)^2 + (b_4 - b_3 c_2 t)^2}. \tag{49}$$

15. Periodic Cross-Rational (PCR) Solutions

We use the following hypothesis [54,55]:

$$f = g_0 + (a_1 \xi + a_2)^2 + (a_3 \xi + a_4)^2 + k_1 \cos(b_1 \xi + b_2) + k_2 \cosh(b_3 \xi + b_4), \tag{50}$$

where a_i and b_i are some constants. Inserting Equation (50) into Equation (34) and solving coefficients of exponential, trigonometric and hyperbolic functions:

Set I.

$$a_1 = a_1, b_3 = \frac{-4\gamma}{3k_2c_1^2}, c_2 = 0, T_r = \frac{3}{4}c_1, b_1 = 0, b_4 = b_4. \tag{51}$$

Using the above values we have:

$$\Delta_{14} = \frac{2e^{i(k_2z)}\left(2a_1(a_2 + a_1(-c_1t + k_1z))^2 + 2a_3(a_4 + a_3(-c_1t + k_1z))^2 - \frac{4\gamma\sinh\left(b_4 - \frac{4(-c_1t+k_1z)\gamma}{3c_1^2k_2}\right)}{3c_1^2}\right)}{g_0 + (a_2 + a_1(-c_1t + k_1z))^2 + (a_4 + a_3(-c_1t + k_1z))^2 + k_2\cosh\left(b_4 - \frac{4(-c_1t+k_1z)\gamma}{3c_1^2k_2}\right)}. \tag{52}$$

16. Result and Discussions

A lot of work has been done on the proposed model: Akhmediev et al. found singularities via a simple approach [56], Soto Crespo et al. studied pulse solutions for the case of normal group-velocity dispersion [57], Yan et al. found stable transmission of solitons for the concerned model via the asymmetric method [58], Biswas et al. worked on Dromion-like structures for the variable-coefficients CQGL-equation by using the asymmetric method [59], Gurevich et al. investigated soliton explosions for the CQGL-equation via explosion modes [60], Uzunov et al. studied pulsating solutions for the CQGL-equation by using the variation method and the method of moments [61], Nikolov et al. interpreted the influence of the higher-order effects on the solutions for the concerned model [62], Mihalache et al. analyzed the coaxial vortex solitons forthe CQGL-Equation [63], Fang et al. worked on soliton dynamics [64], Djoko et al. investigated the effects of the septic nonlinearity [65], Mou et al. studied discrete localized excitations [66] and Liu et al. analyzed harmonic and damped motions of dissipative solitons for the proposed model [67]. However, in this work, we have applied the appropriate transformations method to obtain the stated solutions for the governing model.

This article contains five classes of breather solutions (i.e., MB, KBM, GB, AB and homoclinic breather solutions), as well as lump, lump one stripe, lump two stripe and rogue wave solutions. Furthermore, a detailed analysis of SRW solution is made. Multiwave, M-shaped and interactional solutions are computed for ensuing model. These type of solutions, utilized in diverse fields of sciences, i.e., optics, engineering, physics and biology etc. [11–21]. A breather is a nonlinear localized wave and is a periodic solution of discrete lattice equations. Our newly attained results show a discrepancy of their shapes by appropriate choices of parameters. Now, we can definitely understand the geometric structure from Figure 1, which shows the lump profiles with one bright and dark soliton of the solution Δ_1 in Equation (7) via distinct parameters $\omega = 1$. The bright and dark soliton behavior of three-dimensional profiles steadily increases the value of (i) $a_1 = 5$, (ii) $a_1 = 10$ and (iii) $a_1 = -3$. Figure 2 shows the contour shapes for Figure 1 successively. The lump one stripe profiles of the solution Δ_2 in Equation (10) are interpreted via distinct values of $\omega = 5, k_1 = 2, \rho = 4, \gamma = -1, p = 2, q = -1, \nu = 1$ and $b_0 = 3$. Three-dimensional profiles are shown in Figure 3 at (i) $a_1 = 5$, (ii) $a_1 = 10$ and (iii) $a_1 = -2$. Figure 4 shows the contour shapes for Figure 3 successively. Similarly, Figure 5 shows the lump two stripe graphs of the solution Δ_3 in Equation (13) for the distinct values of $\omega = 5, k_1 = 2, \rho = 4, \gamma = -1, k_2 = 1, k_3 = 1, k_4 = 2$ and $b_0 = 3$, with three-dimensional profiles at (i) $a_0 = 5$, (ii) $a_0 = 10$ and (iii) $a_0 = -2$. Figure 6 builds contour profiles for Figure 5 successively. The MB graphs of the solution Δ_4 in Equation (16) are interpreted via distinct values of $\omega = 5, p_1 = 2, p_2 = 3, \alpha_1 = 1, \alpha_2 = 2.5, \lambda_1 = 1, \lambda_2 = 2, \beta_2 = 3, \rho = 4$ and $\gamma_2 = 1$. Three-dimensional profiles at (i) $a_0 = 5$, (ii) $a_0 = 10$ and (iii) $a_0 = -1$ are shown in Figure 7. Figure 8 shows the contour profiles for Figure 7. In the same way, Figure 9 presents the KMB graphs of solution Δ_5 in Equation (19) through values of $a_1 = 2, a_3 = 1, a_4 = 3, \omega = 5, p_1 = 2, p_2 = 3, b_1 = 1, b_2 = 2.5, b_3 = 1, b_4 = 2$ and $\rho = 4$, with three-dimensional profiles at (i) $a_2 = 5$,

(ii) $a_2 = 20$ and (iii) $a_2 = -1$. Figure 10 shows the contour profiles for Figure 9. The GB profiles of the solution Δ_6 in Equation (24) are formed through values of $\kappa = 5, b = 1$ and $\rho = 4$. Three-dimensional graphs at (i) $\sigma = 0.2$, (ii) $\sigma = 0.8$ and (iii) $\sigma = -0.1$ are shown in Figure 11. Similarly, Figure 12 shows the contour profiles for Figure 11. The AB profiles of the solution Δ_7 in Equation (27) are formed through values of $a = 5$, $b = 1$, $c = 3$, $p_0 = 4$ and $m = 5$. Three-dimensional graphs at (i) $\beta = 5$, (ii) $\beta = 10$ and (iii) $\beta = -3$ are shown in Figure 13, while Figure 14 shows the contour graphs for Figure 13. The SRW profiles of the solution Δ_8 in Equation (30) are constructed for values of $\epsilon = 0.5$, $b = 1$, $c = 3$, $\gamma = 0.1$, $\nu = 10$, $\mu = 2$ and $\kappa = 2$. Three-dimensional graphs at (i) $\delta = -5$, (ii) $\delta = 10$ and (iii) $\delta = 20$ are shown in Figure 14. Figure 15 shows the contour graphs for Figure 14. Similarly, MS graphs of solution Δ_9 in Equation (37) are formed with $a_6 = 0.2$, $c_1 = 1$, $k_1 = 3$, $a_4 = 0.1$, $b_1 = 10$, $b_2 = 2$, $c_2 = 2$ and $k_2 = 3$. Three-dimensional graphs at (i) $a_5 = -5$, (ii) $a_5 = 3$ and (iii) $a_5 = 7$ are shown in Figure 15. Figure 16 shows the contour shapes for Figure 15. The HB profiles of solution Δ_{11} in Equation (43) are constructed for values of $c_1 = 2$, $c_2 = 1$, $k_1 = 3$, $k_2 = 0.1$, $\gamma = 1$ and $\beta = 5$. Three-dimensional graphs at (i) $d_3 = -5$, (ii) $d_3 = 3$ and (iii) $d_3 = 15$ are shown in Figure 17. Figure 18 shows the contour shapes for Figure 17, while the MS profiles of the solution Δ_{11} in Equation (40) are constructed for values of $b_1 = 0.5$, $p = 1$, $a_4 = 3$, $a_2 = 2$, $k_1 = 0.1$, $\nu = 1$ and $T_r = 2$. Three-dimensional graphs at (i) $a_5 = -5$, (ii) $a_5 = 3$ and (iii) $a_5 = 10$ are shown in Figure 19. Figure 20 shows the contour shapes for Figure 19. When the value of a_5 steadily increases, we can see that the waves come closer to interact with each other. In the same manner, Figure 21 presents the soliton profiles of the solution Δ_{12} in Equation (46) for values of $a_4 = 2$, $b_2 = 1$, $b_1 = 3$, $a_2 = 0.1$, $T_r = 1$, $c_2 = 5$, $k_2 = 2$ and $\nu = 3$, with three-dimensional graphs at (i) $a_3 = -5$, (ii) $a_3 = 0.1$ and (iii) $a_5 = 4$. When the value of k_2 steadily increases, we can see from the behavior of the M-shaped wave that the waves come closer to interact with each other. Similarly, Figure 22 shows the contour shapes for Figure 21 successively. The KCR profiles of the solution Δ_{13} in Equation (49) are formed for values of $b_2 = 1$, $b_1 = 3$, $a_2 = 0.1$, $\mu = 2$, $g_0 = 3$, $b_3 = 2$, $b_4 = 5$, $c_2 = 4$ and $k_2 = 2$. Three-dimensional graphs at (i) $a_2 = -5$, (ii) $a_2 = 1$ and (iii) $b_2 = 40$ are shown in Figure 23. Figure 24 shows the contour shapes for Figure 23 successively. The PCR graphs of the solution Δ_{14} in Equation (52) are formed for particular values of $b_2 = 1$, $a_4 = 2$, $a_2 = -3$, $\mu = 2$, $g_0 = 7$, $b_2 = 1$, $c_1 = 3$, $k_1 = 0.1$, $c_2 = 6$, $\gamma = 2$ and $k_2 = 1$. Three-dimensional graphs at (i) $a_1 = -4$, (ii) $a_1 = 0$ and (iii) $a_1 = 30$ are shown in Figure 25. Finally, Figures 26–28 shows the contour shapes for Figure 25 successively.

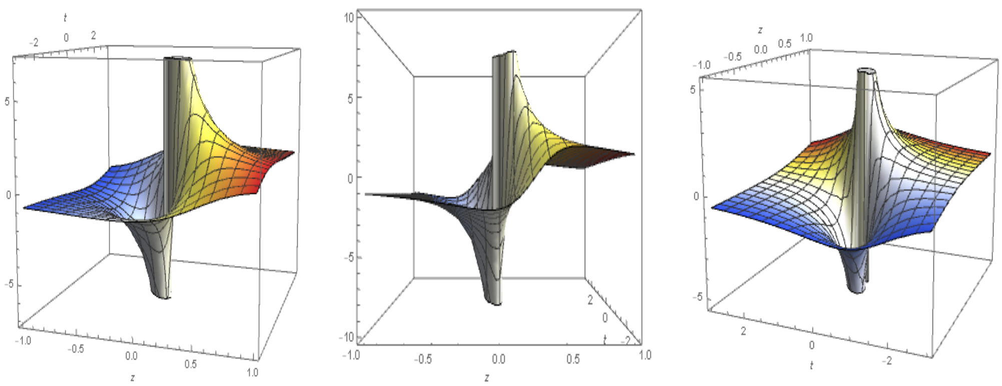

Figure 1. The lump profiles of the solution Δ_1 in Equation (7) are presented via distinct parameters $\omega = 1$. Three-dimensional profiles at (i) $a_1 = 5$, (ii) $a_1 = 10$ and (iii) $a_1 = -3$.

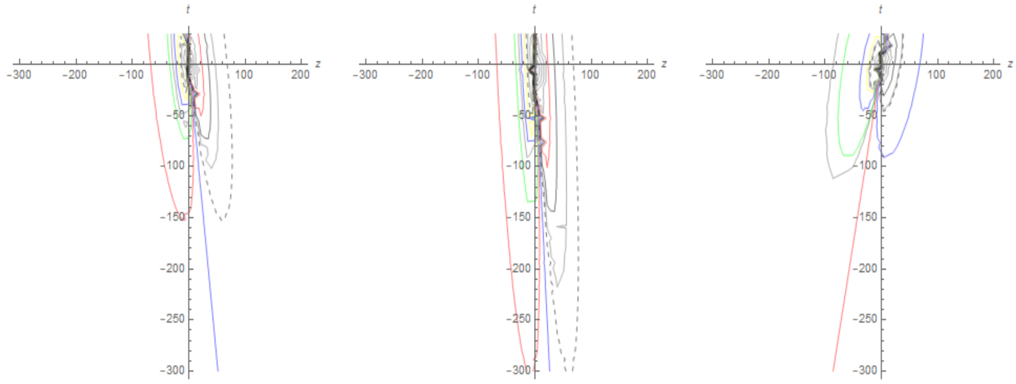

Figure 2. Contours graphs for Figure 1.

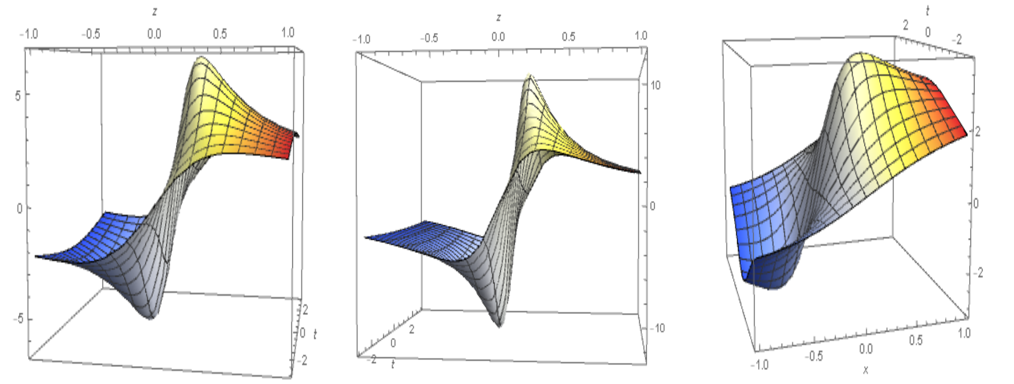

Figure 3. The lump one stripe profiles of the solution Δ_2 in Equation (10) are interpreted via distinct values of $\omega = 5, k_1 = 2, \rho = 4, \gamma = -1, p = 2, q = -1, \nu = 1, b_0 = 3$. Three-dimensional profiles are shown in (i) $a_1 = 5$, (ii) $a_1 = 10$ and (iii) $a_1 = -2$.

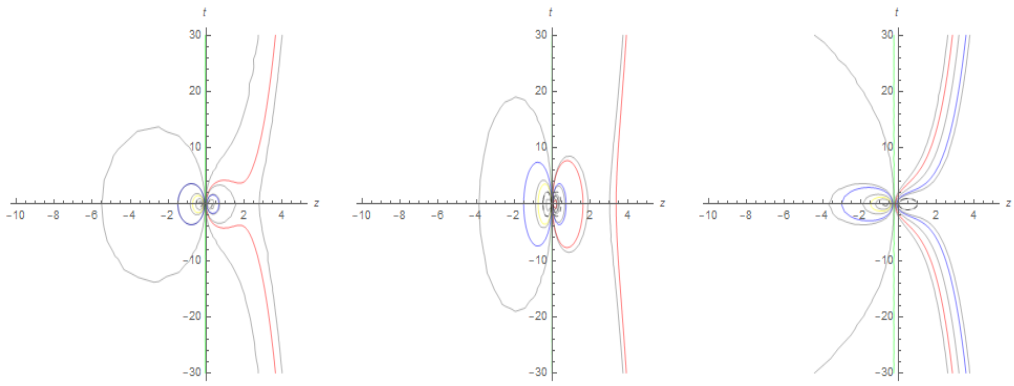

Figure 4. Contour displays for Figure 3.

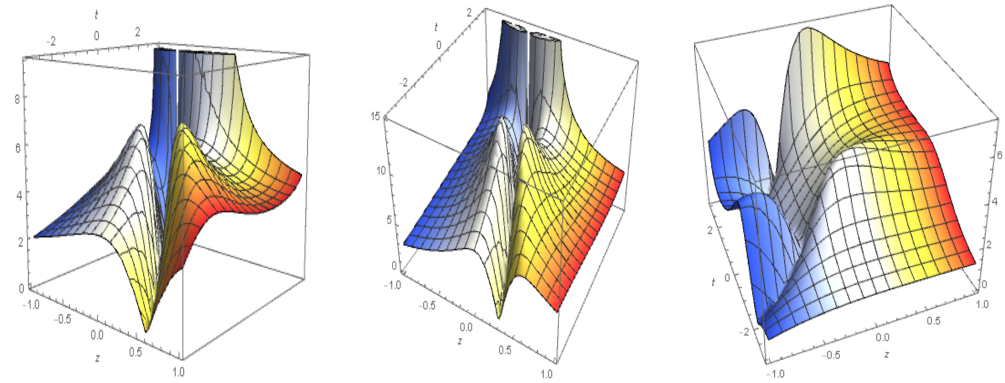

Figure 5. The lump two stripe graphs of the solution Δ_3 in Equation (13) are interpreted via distinct values of $\omega = 5$, $k_1 = 2$, $\rho = 4$, $\gamma = -1$, $k_2 = 1$, $k_3 = 1$, $k_4 = 2$, $b_0 = 3$. Three-dimensional profiles at (i) $a_0 = 5$, (ii) $a_0 = 10$ and (iii) $a_0 = -2$.

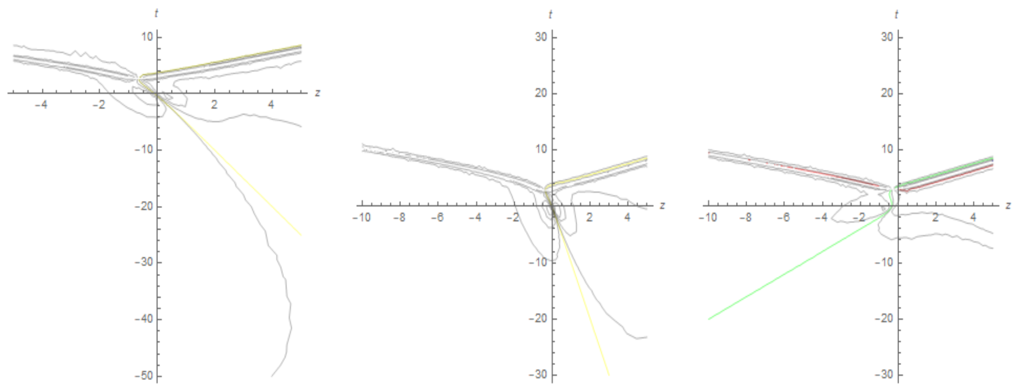

Figure 6. Contour graphs for Figure 5.

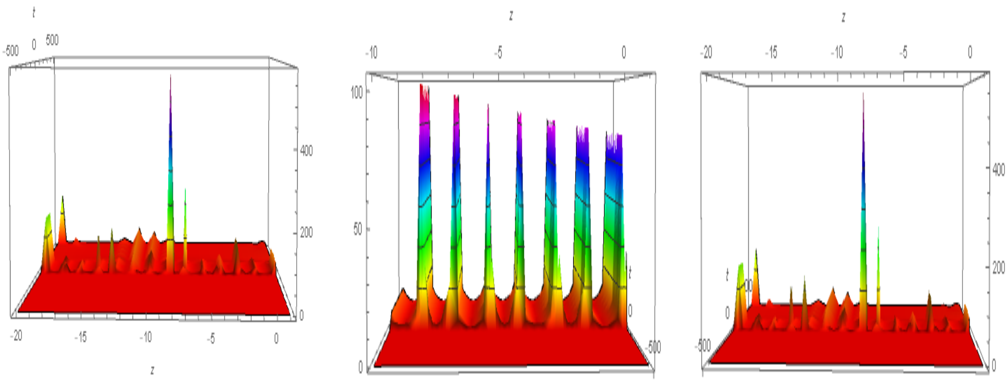

Figure 7. The MB graphs of the solution Δ_4 in Equation (16) are interpreted via distinct values of $\omega = 5$, $p_1 = 2$, $p_2 = 3$, $\alpha_1 = 1$, $\alpha_2 = 2.5$, $\lambda_1 = 1$, $\lambda_2 = 2$, $\beta_2 = 3$, $\rho = 4$, $\gamma_2 = 1$. Three-dimensional profiles at (i) $a_0 = 5$, (ii) $a_0 = 10$ and (iii) $a_0 = -1$.

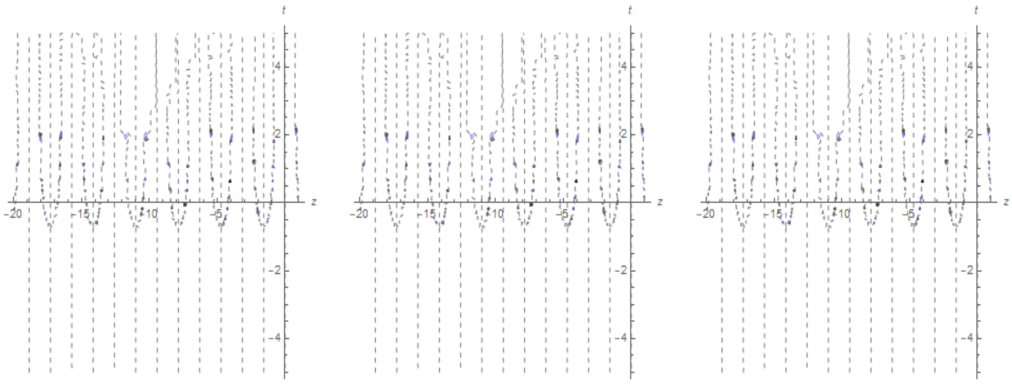

Figure 8. Contour graphs for Figure 7.

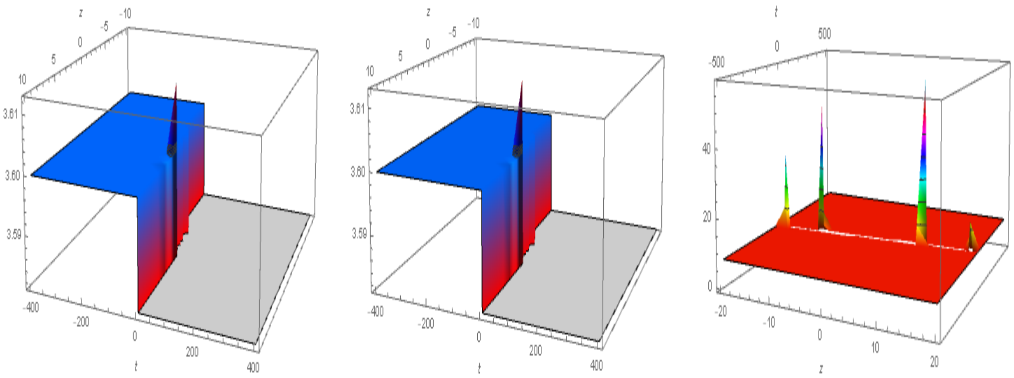

Figure 9. The KMB graphs of the solution Δ_5 in Equation (19) are interpreted through values of $a_1 = 2$, $a_3 = 1$, $a_4 = 3$, $\omega = 5$, $p_1 = 2$, $p_2 = 3$, $b_1 = 1$, $b_2 = 2.5$, $b_3 = 1$, $b_4 = 2$ and $\rho = 4$. Three-dimensional profiles at (i) $a_2 = 5$, (ii) $a_2 = 20$ and (iii) $a_2 = -1$.

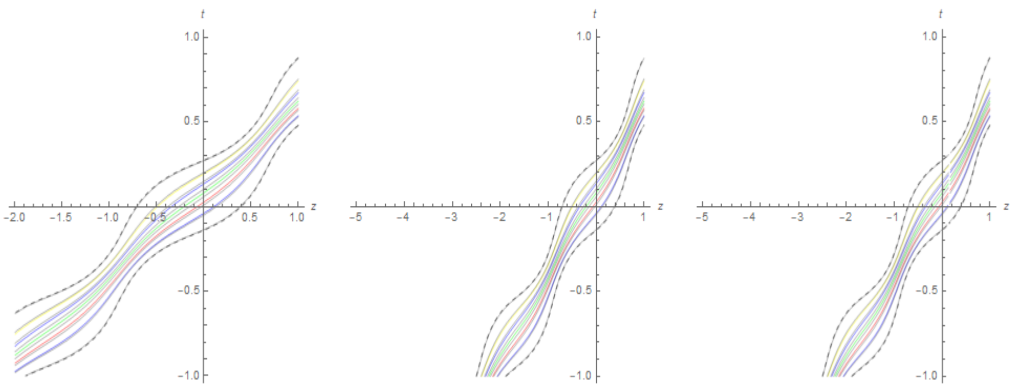

Figure 10. Contour graphs for Figure 9.

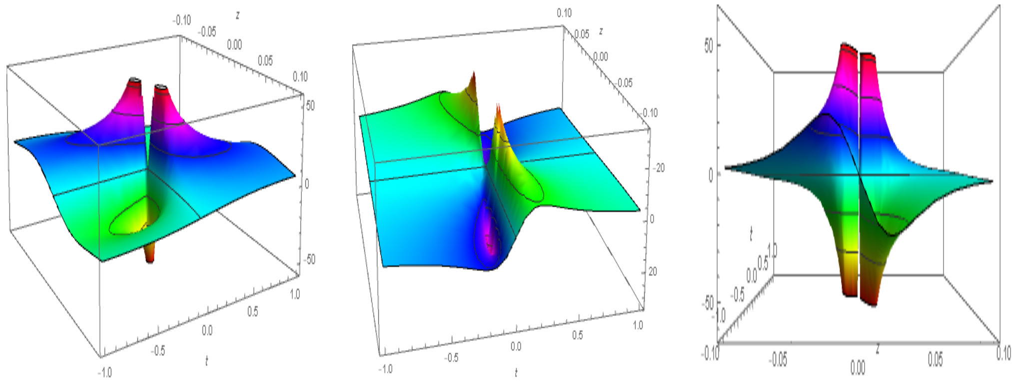

Figure 11. The GB profiles of the solution Δ_6 in Equation (24) are made through values of $\kappa = 5$, $b = 1$ and $\rho = 4$. Three-dimensional graphs at (i) $\sigma = 0.2$, (ii) $\sigma = 0.8$ and (iii) $\sigma = -0.1$.

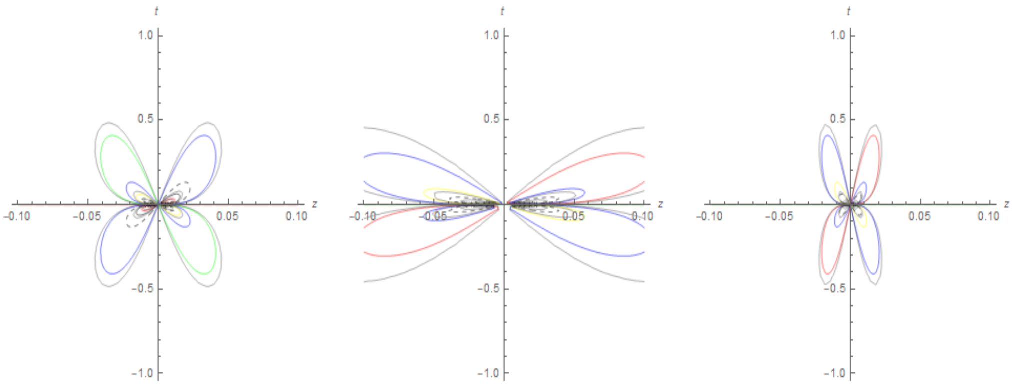

Figure 12. Contour graphs for Figure 11.

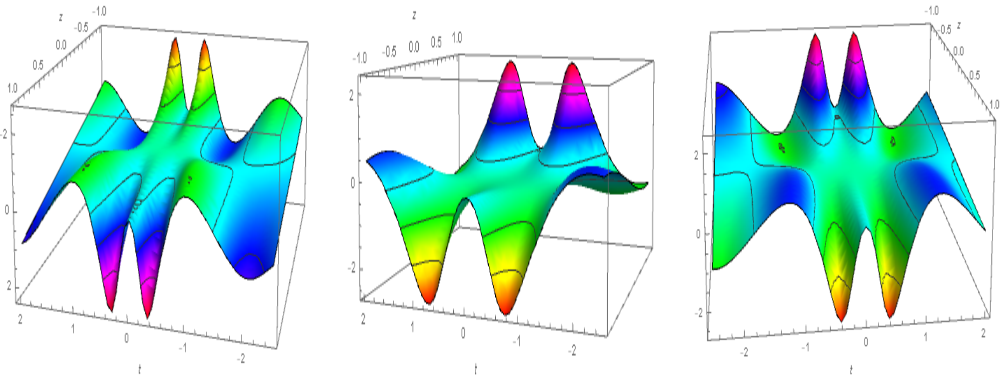

Figure 13. The AB profiles of the solution Δ_7 in Equation (27) are made through values of $a = 5$, $b = 1$, $c = 3$, $p_0 = 4$ and $m = 5$. Three-dimensional graphs at (i) $\beta = 5$, (ii) $\beta = 10$ and (iii) $\beta = -3$.

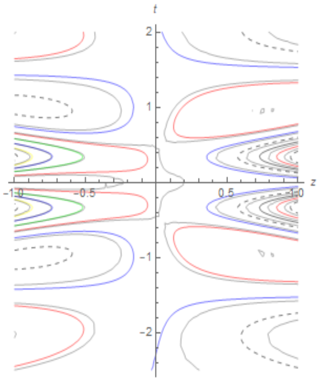

Figure 14. Contour slots for Figure 13.

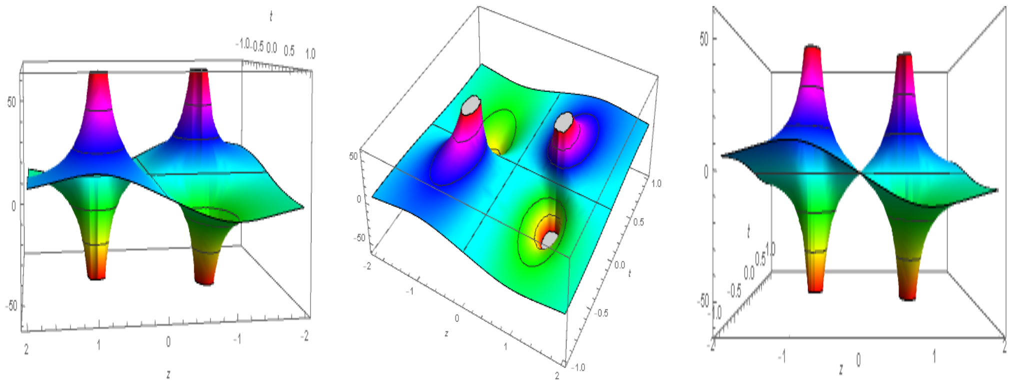

Figure 15. The SRW profiles of the solution Δ_8 in Equation (30) are made for values of $\epsilon = 0.5$, $b = 1$, $c = 3$, $\gamma = 0.1$, $\nu = 10$, $\mu = 2$ and $\kappa = 2$. Three-dimensional graphs at (i) $\delta = -5$, (ii) $\delta = 10$ and (iii) $\delta = 20$.

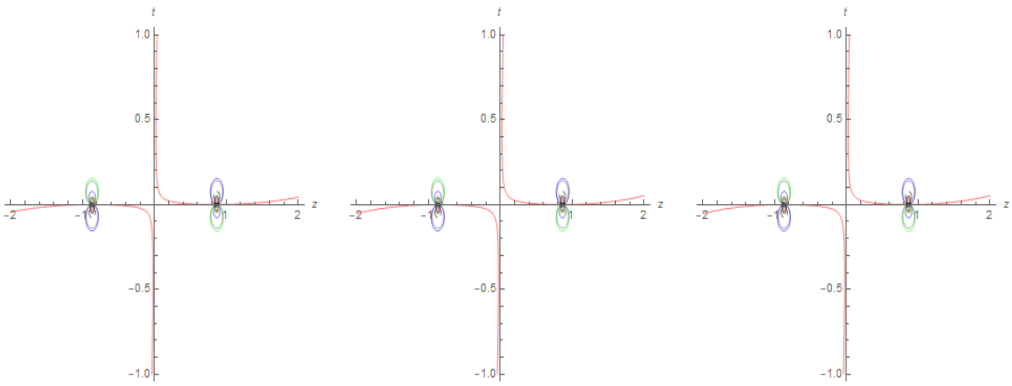

Figure 16. Contour slots for Figure 15.

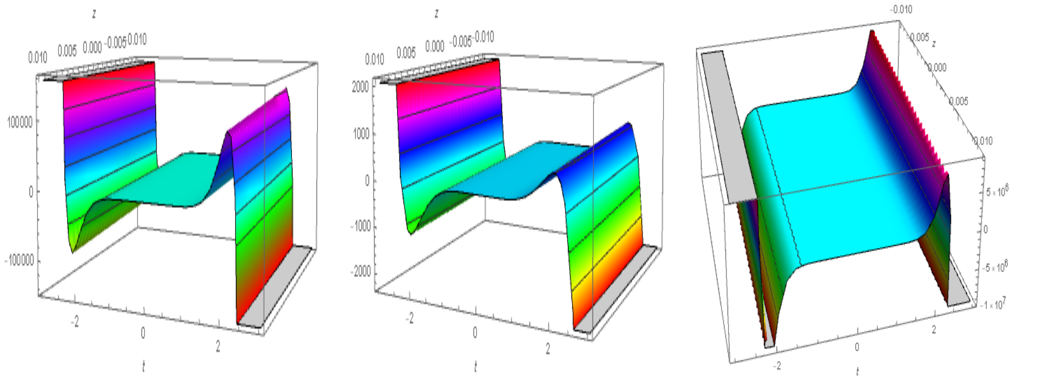

Figure 17. The MS graphs of the solution Δ_9 in Equation (37) are made for values of $a_6 = 0.2$, $c_1 = 1$, $k_1 = 3, a_4 = 0.1, b_1 = 10, b_2 = 2, c_2 = 2, k_2 = 3$. Three-dimensional graphs at (i) $a_5 = -5$, (ii) $a_5 = 3$ and (iii) $a_5 = 7$.

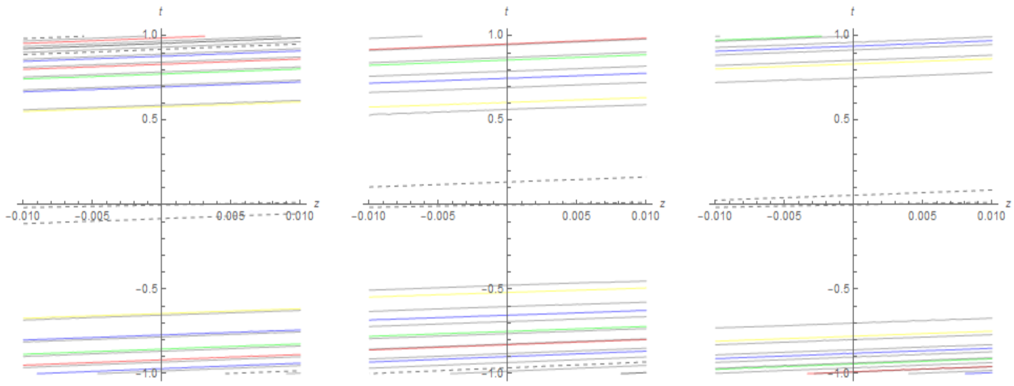

Figure 18. Contour slots for Figure 17.

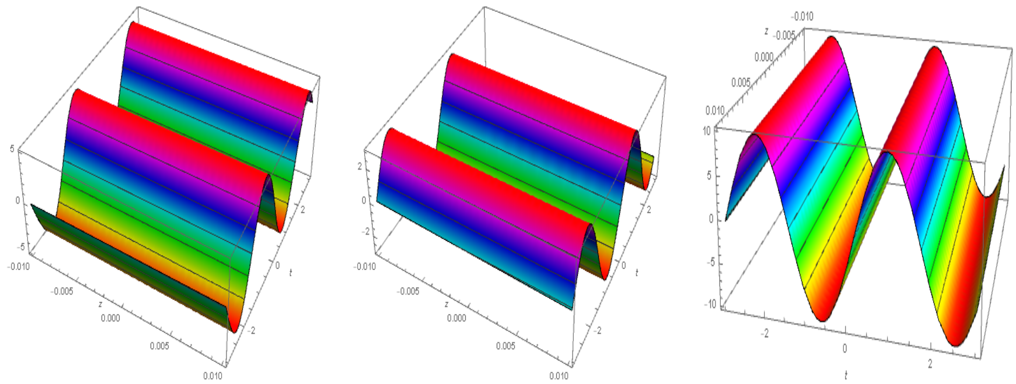

Figure 19. The HB profiles of the solution Δ_{11} in Equation (43) are constructed for values of $c_1 = 2$, $c_2 = 1$, $k_1 = 3$, $k_2 = 0.1$, $\gamma = 1$ and $\beta = 5$. Three-dimensional graphs at (i) $d_3 = -5$, (ii) $d_3 = 3$ and (iii) $d_3 = 15$.

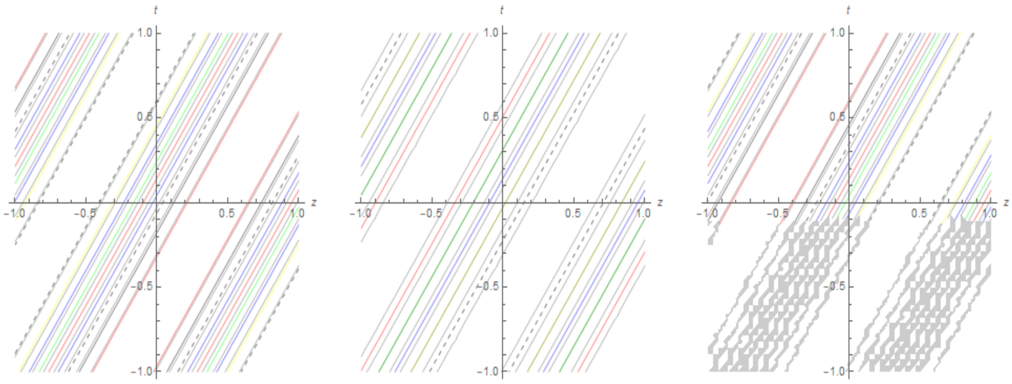

Figure 20. Contour slots for Figure 19.

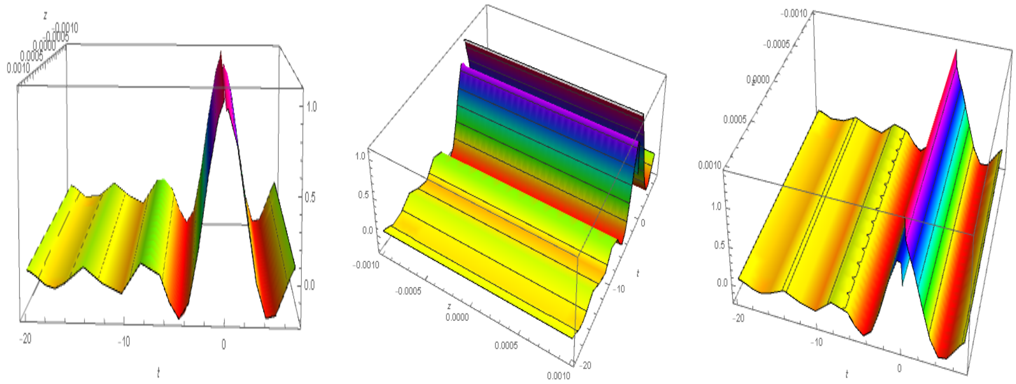

Figure 21. The MS profiles of the solution Δ_{11} in Equation (40) are constructed for values of $b_1 = 0.5$, $p = 1$, $a_4 = 3$, $a_2 = 2$, $k_1 = 0.1$, $\nu = 1$ and $T_r = 2$. Three-dimensional graphs at (i) $a_5 = -5$, (ii) $a_5 = 3$ and (iii) $a_5 = 10$.

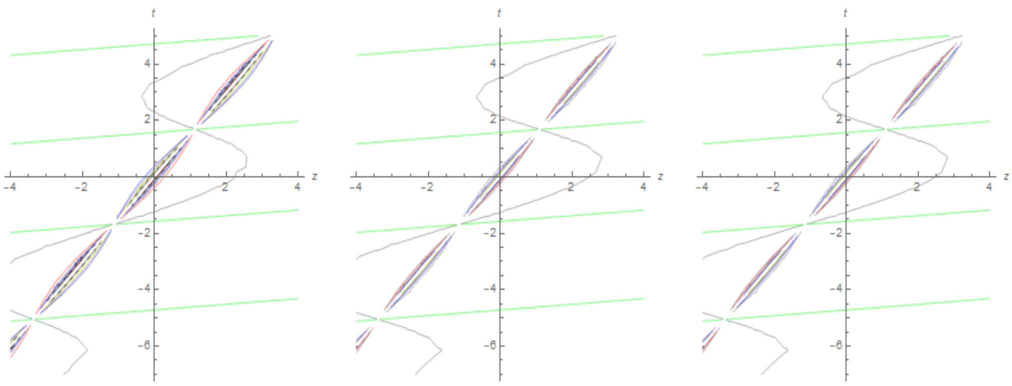

Figure 22. Contour slots for Figure 21.

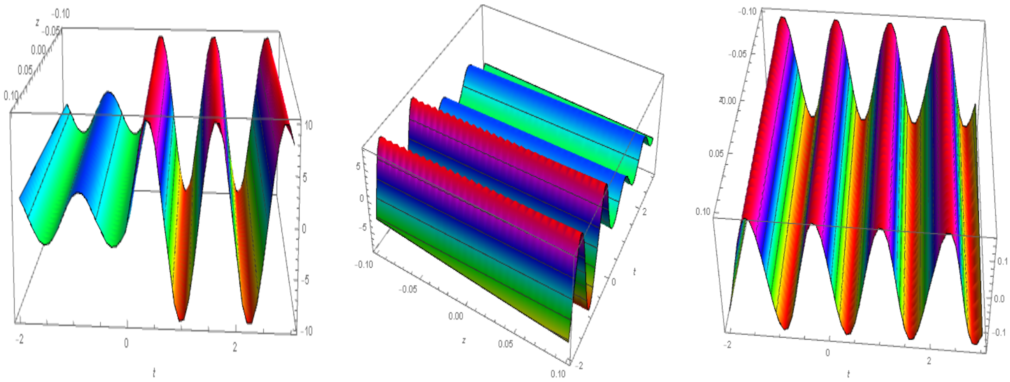

Figure 23. The soliton profiles of the solution Δ_{12} in Equation (46) are made for values of $a_4 = 2$, $b_2 = 1$, $b_1 = 3$, $a_2 = 0.1$, $T_r = 1$, $c_2 = 5$, $k_2 = 2$ and $\nu = 3$. Three-dimensional graphs at (i) $a_3 = -5$, (ii) $a_3 = 0.1$ and (iii) $a_5 = 4$.

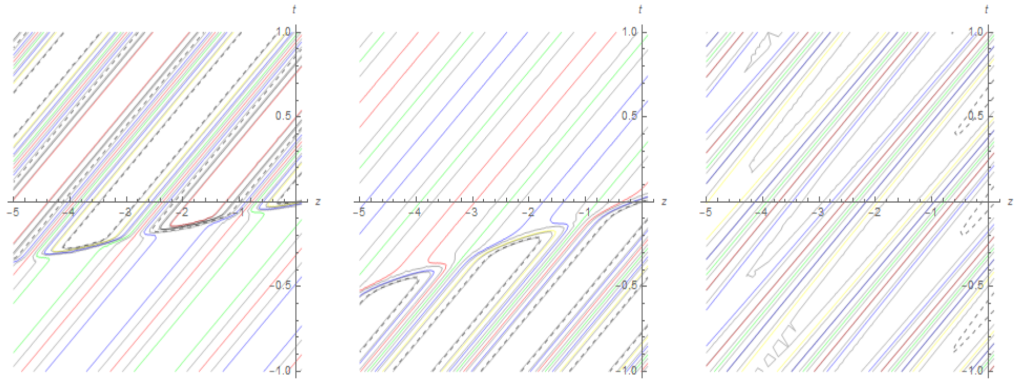

Figure 24. Contour profiles for Figure 23.

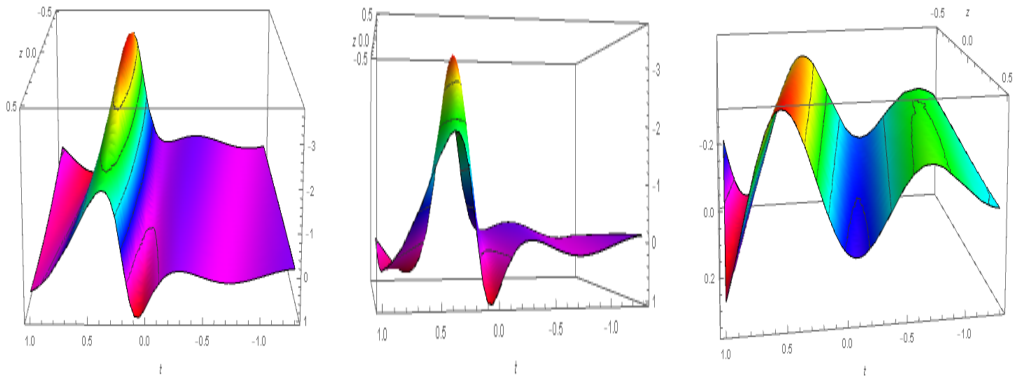

Figure 25. The KCR profiles of the solution Δ_{13} in Equation (49) are formed for values of $b_2 = 1$, $b_1 = 3$, $a_2 = 0.1$, $\mu = 2$, $g_0 = 3$, $b_3 = 2$, $b_4 = 5$, $c_2 = 4$ and $k_2 = 2$. Three-dimensional graphs at (i) $a_2 = -5$, (ii) $a_2 = 1$ and (iii) $b_2 = 40$.

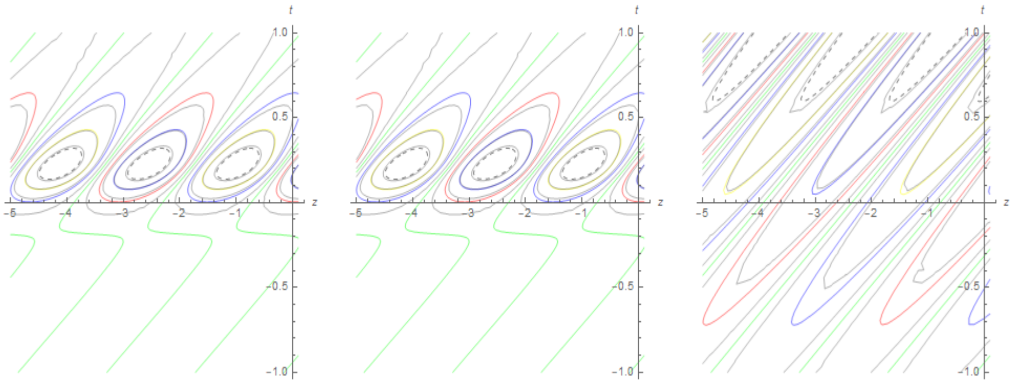

Figure 26. Contour profiles for Figure 25.

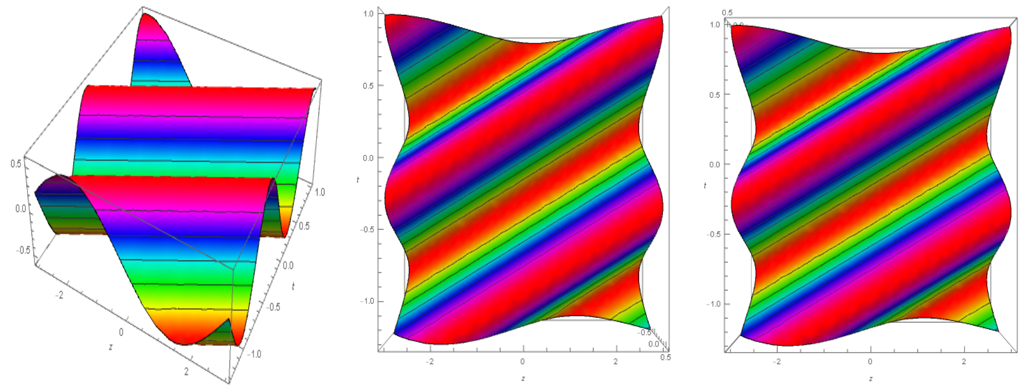

Figure 27. The PCR graphs of the solution Δ_{14} in Equation (52) are formed for particular values of $b_2 = 1$, $a_4 = 2$, $a_2 = -3$, $\mu = 2$, $g_0 = 7$, $b_2 = 1$, $c_1 = 3$, $k_1 = 0.1$, $c_2 = 6$ and $\gamma = 2, k_2 = 1$. Three-dimensional graphs at (i) $a_1 = -4$, (ii) $a_1 = 0$ and (iii) $a_1 = 30$.

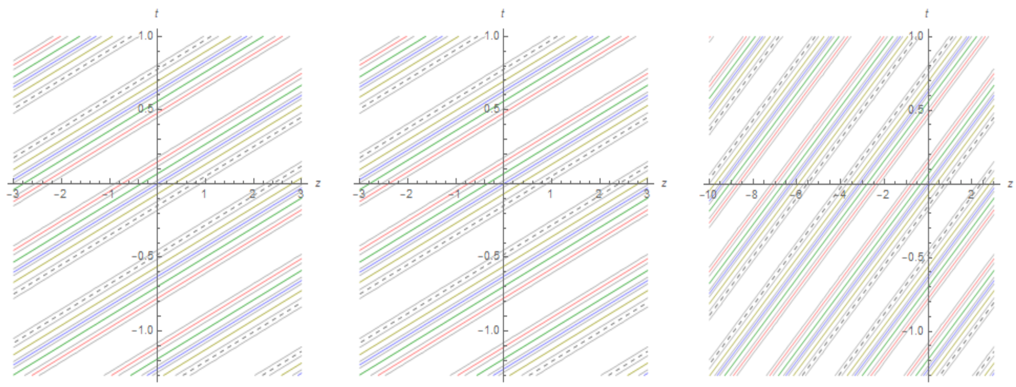

Figure 28. Shows contour shapes for Figure 27.

17. Concluding Remarks

We have considered the CQGL-equation under the influence of intrapulse Raman scattering (IRS) and constructed distinct localized wave solutions by employing test functions with the aid of an appropriate transformations method. Five classes of breather solutions (i.e., Ma, Kuznetsov-Ma, GB, AB, homoclinic breather solutions), as well as lump, lump one stripe, lump two stripe and rogue wave solutions were successfully evaluated. Furthermore, a detailed analysis of SRW solution was performed. Multiwave, *M*-shaped, interactional solutions, KCR solutions and PCR solutions are computed for the ensuing model. Interaction behaviors between multiple-lump waves and soliton were also discussed. Multiple-lump wave evolution with time was also observed. We graphically presented many valuable results obtained here. The conditions imposed on the parameters have been explicitly demonstrated to guarantee that they were well defined and that the solutions were localized. To our knowledge, the results are new for the governing equation. These results may be useful for the experimental realization of undistorted transmission of optical waves in optical fibers and further understanding of their optical transmission properties. Finally, we hope that the exact nature of these solitary waves interpreted here may be profitably exploited in designing the optimal Raman fiber laser experiments.

Author Contributions: Conceptualization, A.R.S. and S.T.R.R.; methodology, A.R.S.; software, S.T.R.R.; validation, H.Z., S.T.R.R.; formal analysis, S.T.R.R.; investigation, A.R.S.; writing—original draft preparation, S.T.R.R.; writing—review and editing, A.R.S.; visualization, S.T.R.R.; supervision, A.R.S.; project administration, H.Z.; funding acquisition, H.Z. All authors have read and agreed to the published version of the manuscript.

Funding: Deputyship for Research and Innovation, Ministry of Education in Saudi Arabia for funding this research work the project number (141/442).

Institutional Review Board Statement: Not applicable.

Informed Consent Statement: Not applicable.

Data Availability Statement: Not applicable.

Acknowledgments: The authors extend their appreciation to the Deputyship for Research and Innovation, Ministry of Education in Saudi Arabia for funding this research work the project number (141/442). Furthermore, the authors would like to extend their appreciation to Taibah University for its supervision support.

Conflicts of Interest: The authors declare no conflict of interest.

References

1. Kumar, S.; Kumar, D.; Kharbanda, H. Lie symmetry analysis, abundant exact solutions and dynamics of multisolitons to the (2 + 1)-dimensional KP-BBM equation. *Pramana* **2021**, *95*, 33. [CrossRef]
2. Kumar, S.; Kumar, D. Lie symmetry analysis and dynamical structures of soliton solutions for the (2 + 1)-dimensional modified CBS equation. *Int. J. Mod. Phys. B* **2020**, *34*, 2050221. [CrossRef]
3. Kumar, S.; Kumar, A. Lie symmetry reductions and group invariant solutions of (2 + 1)-dimensional modified Veronese web equation. *Nonlinear Dyn.* **2019**, *98*, 1891–1903. [CrossRef]
4. Kumar, S.; Niwas, M.; ; Wazwaz, A.M. Lie symmetry analysis, exact analytical solutions and dynamics of solitons for (2 + 1)-dimensional NNV equations. *Phys. Scr.* **2020**, *95*, 095204. [CrossRef]
5. Kumar, S.; Rani, S. Lie symmetry reductions and dynamics of soliton solutions of (2 + 1)-dimensional Pavlov equation. *Pramana* **2020**, *94*, 116. [CrossRef]
6. Kudryashov, N.A. The generalized Duffing oscillator. *Commun. Nonlinear Sci. Numer. Simul.* **2021**, *93*, 105526. [CrossRef]
7. Kudryashov, N.A. Model of propagation pulses in an optical fiber with a new law of refractive indices. *Optik* **2021**, *248*, 168160. [CrossRef]
8. Kudryashov, N.A. Solitary waves of the non-local Schrödinger equation with arbitrary refractive index. *Optik* **2021**, *231*, 166443. [CrossRef]
9. Kudryashov, N.A. Almost general solution of the reduced higher-order nonlinear Schrödinger equation. *Optik* **2021**, *230*, 166347. [CrossRef]
10. Kudryashov, N.A. Periodic and solitary waves in optical fiber Bragg gratings with dispersive reflectivity. *Chin. J. Phys.* **2020**, *66*, 401–405. [CrossRef]
11. Younas, U.; Younis, M.; Seadawy, A.R.; Rizvi, S.T.R.; Althobaiti, S.; Sayed, S. Diverse exact solutions for modified nonlinear Schrödinger equation with conformable fractional derivative. *Results Phys.* **2021**, *20*, 103766. [CrossRef]
12. Akram, U.; Seadawy, A.R.; Rizvi, S.T.R.; Younis, M.; Althobaiti, S.; Sayed, S. Traveling wave solutions for the fractional Wazwaz–Benjamin–Bona–Mahony model in arising shallow water waves. *Results Phys.* **2021**, *20*, 103725. [CrossRef]
13. Seadawy, A.R.; Bilal, M.; Younis, M.; Rizvi, S.T.R.; Althobaiti, S.; Makhlouf, M.M. Analytical mathematical approaches for the double-chain model of DNA by a novel computational technique. *Chaos Solitons Fractals* **2021**, *144*, 110669. [CrossRef]
14. Seadawy, A.R.; Rehman, S.U.; Younis, M.; Rizvi, S.T.R.; Althobaiti, S.; Makhlouf, M.M. Modulation instability analysis and longitudinal wave propagation in an elastic cylindrical rod modelled with Pochhammer-Chree equation. *Phys. Scr.* **2021**, *96*, 045202. [CrossRef]
15. Seadawy, A.R.; Rizvi, S.T.R.; Ahmad, S.; Younis, M.; Baleanu, D. Lump, lump-one stripe, multiwave and breather solutions for the Hunter–Saxton equation. *Open Phys.* **2021**, *19*, 1–10. [CrossRef]

16. Bilal, M.; Seadawy, A.R.; Younis, M.; Rizvi, S.T.R.; El-Rashidy, K.; Mahmoud, S.F. Analytical wave structures in plasma physics modelled by Gilson-Pickering equation by two integration norms. *Results Phys.* **2021**, *23*, 103959. [CrossRef]
17. Rizvi, S.T.R.; Seadawy, A.R.; Younis, M.; Ali, I.; Althobaiti, S.; Mahmoud, S.F. Soliton solutions, Painleve analysis and conservation laws for a nonlinear evolution equation. *Results Phys.* **2021**, *23*, 103999. [CrossRef]
18. Rizvi, S.T.R.; Seadawy, A.R.; Younis, M.; Iqbal, S.; Althobaiti, S.; El-Shehawi, A.M. Various optical soliton for a weak fractional nonlinear Schrödinger equation with parabolic law. *Results Phys.* **2021**, *23*, 103998. [CrossRef]
19. Seadawy, A.R.; Rizvi, S.T.; Ali, I.; Younis, M.; Ali, K.; Makhlouf, M.M.; Althobaiti, A. Conservation laws, optical molecules, modulation instability and Painlevé analysis for the Chen–Lee–Liu model. *Opt. Quantum Electron.* **2021**, *53*, 172. [CrossRef]
20. Tariq, K.U.; Zainab, H.; Seadawy, A.R.; Younis, M.; Rizvi, S.T.R.; Abd Allah, A.M. On some novel optical wave solutions to the paraxial M-fractional nonlinear Schrödinger dynamical equation. *Opt. Quantum Electron.* **2021**, *53*, 219. [CrossRef]
21. Ahmed, S.; Ashraf, R.; Seadawy, A.R.; Rizvi, S.T.R.; Younis, M.; Althobaiti, A.; El-Shehawi, A.M. Lump, multi-wave, kinky breathers, interactional solutions and stability analysis for general $(2+1)$-rth dispersionless Dym equation. *Results Phys.* **2021**, *25*, 104160. [CrossRef]
22. Maan, N.; Goyal, A.; Raju, T.S.; Kumar, C.N. Chirped Lambert W-kink solitons of the complex cubic-quintic Ginzburg-Landau equation with intrapulse Raman scattering. *Phys. Lett. A* **2020**, *384*, 126675.
23. Kumar, S.; Kumar, D.; Kumar, A. Lie symmetry analysis for obtaining the abundant exact solutions, optimal system and dynamics of solitons for a higher-dimensional Fokas equation. *Chaos Solitons Fractals* **2021**, *142*, 110507. [CrossRef]
24. Gao, X.Y.; Guo, Y.J.; Shan, W.R.; Yuan, Y.Q.; Zhang, C.R.; Chen, S.S. Magneto-optical/ferromagnetic-material computation: Bäcklund transformations, bilinear forms and N solitons for a generalized $(3+1)$-dimensional variable-coefficient modified Kadomtsev–Petviashvili system. *Appl. Math. Lett.* **2021**, *111*, 106627. [CrossRef]
25. Li, P.; Li, R.; Dai, C. Existence, symmetry breaking bifurcation and stability of two-dimensional optical solitons supported by fractional diffraction. *Opt. Express* **2021**, *29*, 3193–3210. [CrossRef]
26. Xu, G.; Nielsen, A.U.; Garbin, B.; Hill, L.; Oppo, G.L.; Fatome, J.; Erkintalo, M. Spontaneous symmetry breaking of dissipative optical solitons in a two-component Kerr resonator. *Nat. Commun.* **2021**, *12*, 4023. [CrossRef] [PubMed]
27. Kaur, L.; Wazwaz, A.M. Einstein's vacuum field equation: Painlevé analysis and Lie symmetries. *Waves Random Complex Media* **2021**, *31*, 199–206. [CrossRef]
28. Noeiaghdam, S.; Sidorov, D.; Wazwaz, A.M.; Sidorov, N.; Sizikov, V. The Numerical Validation of the Adomian Decomposition Method for Solving Volterra Integral Equation with Discontinuous Kernels Using the CESTAC Method. *Mathematics* **2021**, *9*, 260. [CrossRef]
29. Seadawy, A.R.; Ahmed, H.M.; Rabie, W.B.; Biswas, A. Chirp-free optical solitons in fiber Bragg gratings with dispersive reflectivity having polynomial law of nonlinearity. *Optik* **2021**, *225*, 165681. [CrossRef]
30. He, J.H. Variational principle and periodic solution of the Kundu-Mukherjee-Naskar equation. *Results Phys.* **2020**, *17*, 103031. [CrossRef]
31. Wazwaz, A.M. The Hirota bilinear method and the tanh–coth method for multiple-soliton solutions of the Sawada–Kotera–Kadomtsev–Petviashvili equation. *Appl. Math. Comput.* **2008**, *200*, 160–166.
32. Seadawy, A.R.; Cheemaa, N. Applications of extended modified auxiliary equation mapping method for high-order dispersive extended nonlinear Schrödinger equation in nonlinear optics. *Mod. Phys. Lett. B* **2019**, *33*, 1950203. [CrossRef]
33. Farah, N.; Seadawy, A.R.; Ahmad, S.; Rizvi, S.T.R.; Younis, M. Interaction properties of soliton molecules and Painleve analysis for nano bioelectronics transmission model. *Opt. Quantum Electron.* **2020**, *52*, 329. [CrossRef]
34. Gaber, A.A.; Aljohani, A.F.; Ebaid, A.; Machado, J.T. The generalized Kudryashov method for nonlinear space–time fractional partial differential equations of Burgers type. *Nonlinear Dyn.* **2019**, *95*, 361–368 [CrossRef]
35. Rizvi, S.T.R.; Ali, K.; Ahmad, M. Optical solitons for Biswas–Milovic equation by new extended auxiliary equation method. *Optik* **2020**, *204*, 164181. [CrossRef]
36. Ghaffar, A.; Ali, A.; Ahmed, S.; Akram, S.; Baleanu, D.; Nisar, K.S. A novel analytical technique to obtain the solitary solutions for nonlinear evolution equation of fractional order. *Adv. Differ. Equ.* **2020**, *2020*, 308. [CrossRef]
37. Bashir, A.; Seadawy, A.R.; Rizvi, S.T.R.; Younis, M.; Ali, I.; Abd Allah, A.M. Application of scaling invariance approach, P-test and soliton solutions for couple of dynamical models. *Results Phys.* **2021**, *25*, 104227. [CrossRef]
38. Seadawy, A.R.; Bilal, M.; Younis, M.; Rizvi, S.T.R.; Makhlouf, M.M.; Althobaiti, S. Optical solitons to birefringent fibers for coupled Radhakrishnan–Kundu–Lakshmanan model without four-wave mixing. *Opt. Quantum Electron.* **2021**, *53*, 324. [CrossRef]
39. Yusuf, A.; Inc, M.; Aliyu, A.I.; Baleanu, D. Efficiency of the new fractional derivative with nonsingular Mittag–Leffler kernel to some nonlinear partial differential equations. *Chaos Solitons Fractals* **2018**, *116*, 220–226. [CrossRef]
40. Merabti, A.; Triki, H.; Azzouzi, F.; Zhou, Q.; Biswas, A.; Liu, W.; Abdessetar, E.A. Propagation properties of chirped optical similaritons with dual-power law nonlinearity. *Chaos Solitons Fractals* **2020**, *140*, 110158.
41. Celik, N.; Seadawy, A.R.; Ozkan, Y.S.; Yaşar, E. A model of solitary waves in a nonlinear elastic circular rod: Abundant different type exact solutions and conservation laws. *Chaos Solitons Fractals* **2021**, *143*, 110486. [CrossRef]
42. Rizvi, S.T.R.; Seadawy, A.R.; Ahmed, S.; Younis, M.; Ali, K. Lump, rogue wave, multi-waves and Homoclinic breather solutions for $(2+1)$-Modified Veronese Web equation. *Int. J. Mod. Phys. B* **2021**, *35*, 2150055. [CrossRef]
43. Zhou, Y.; Manukure, S.; Ma, W.X. Lump and lump-soliton solutions to the Hirota Satsuma equation. *Commun. Nonlinear Sci. Numer. Simul.* **2019**, *68*, 56–62. [CrossRef]

44. Wang, H. Lump and interaction solutions to the $(2+1)$-dimensional Burgers equation. *Appl. Math. Lett.* **2018**, *85*, 27–34. [CrossRef]
45. Wu, P.; ; Zhang, Y.; Muhammad, I.; Yin, Q. Lump, periodic lump and interaction lump stripe solutions to the $(2+1)$-dimensional B-type Kadomtsev–Petviashvili equation. *Mod. Phys. Lett. B* **2018**, *32*, 1850106. [CrossRef]
46. Li, B.Q.; Ma, Y.L. multiple-lump waves for a $(3+1)$-dimensional Boiti–Leon–Manna–Pempinelli equation arising from incompressible fluid. *Comput. Math. Appl.* **2018**, *76*, 204–214. [CrossRef]
47. Yu, M.; Jang, J.K.; Okawachi, Y.; Griffith, A.G.; Luke, K.; Miller, S.A.; Gaeta, A.L. Breather soliton dynamics in microresonators. *Nat. Commun.* **2017**, *8*, 14569. [CrossRef] [PubMed]
48. Ahmed, I.; Seadawy, A.R.; Lu, D. Kinky breathers, W-shaped and multi-peak solitons interaction in $(2+1)$-dimensional nonlinear Schrödinger equation with Kerr law of nonlinearity. *Eur. Phys. J. Plus* **2019**, *134*, 120. [CrossRef]
49. Liu, Y.; Li, B.; Wazwaz, A.M. Novel high-order breathers and rogue waves in the Boussinesq equation via determinants. *Int. J. Mod. Phys. B* **2020**, *43*, 3701–3715. [CrossRef]
50. Lu, X.; Chen, S.J. Interaction solutions to nonlinear partial differential equations via Hirota bilinear forms: One-lump-multi-stripe and one-lump-multi-soliton types. *Nonlinear Dyn.* **2021**, *103*, 947–977. [CrossRef]
51. Singh, S.; Sakkaravarthi, K.; Murugesan, K.; Sakthivel, R. Benjamin-Ono equation: Rogue waves, generalized breathers, soliton bending, fission, and fusion. *Eur. Phys. J. Plus* **2020**, *135*, 823. [CrossRef]
52. Dudley, J.M.; Genty, G.; Dias, F.; Kibler, B.; Akhmediev, N. Modulation instability, Akhmediev Breathers and continuous wave supercontinuum generation. *Opt. Express* **2009**, *17*, 21497–21508. [CrossRef]
53. Ahmed, I.; Seadawy, A.R.; Lu, D. *M*-shaped rational solitons and their interaction with kink waves in the Fokas–Lenells equation. *Phys. Scr.* **2019**, *94*, 055205. [CrossRef]
54. Seadawy, A.R.; Rizvi, S.T.; Ashraf, M.A.; Younis, M.; Hanif, M. Rational solutions and their interactions with kink and periodic waves for a nonlinear dynamical phenomenon. *Int. J. Mod. Phys. B* **2021**, *35*, 2150236. [CrossRef]
55. Manafian, J.; Mohammadi Ivatloo, B.; Abapour, M. Breather wave, periodic, and cross-kink solutions to the generalized Bogoyavlensky-Konopelchenko equation. *Math. Methods Appl. Sci.* **2020**, *43*, 1753–1774. [CrossRef]
56. Akhmediev, N.N.; Afanasjev, V.V.; Soto-Crespo, J.M. Singularities and special soliton solutions of the cubic-quintic complex Ginzburg-Landau equation. *Phys. Rev. E* **1996**, *53*, 1190. [CrossRef]
57. Soto-Crespo, J.M.; Akhmediev, N.N.; Afanasjev, V.V.; Wabnitz, S. Pulse solutions of the cubic-quintic complex Ginzburg-Landau equation in the case of normal dispersion. *Phys. Rev. E* **1997**, *55*, 4783. [CrossRef]
58. Yan, Y.; Liu, W. Stable transmission of solitons in the complex cubic–quintic Ginzburg–Landau equation with nonlinear gain and higher-order effects. *Appl. Math. Lett.* **2019**, *98*, 171–176. [CrossRef]
59. Yan, Y.; Liu, W.; Zhou, Q.; Biswas, A. Dromion-like structures and periodic wave solutions for variable-coefficients complex cubic–quintic Ginzburg–Landau equation influenced by higher-order effects and nonlinear gain. *Nonlinear Dyn.* **2020**, *99*, 1313–1319. [CrossRef]
60. Gurevich, S.V.; Schelte, C.; Javaloyes, J. Impact of high-order effects on soliton explosions in the complex cubic-quintic Ginzburg Landau equation. *Phys. Rev. A* **2019**, *99*, 061803. [CrossRef]
61. Uzunov, I.M.; Georgiev, Z.D.; Arabadzhiev, T.N. Transitions of stationary to pulsating solutions in the complex cubic-quintic Ginzburg-Landau equation under the influence of nonlinear gain and higher-order effects. *Phys. Rev. E* **2018**, *97*, 052215. [CrossRef] [PubMed]
62. Uzunov, I.M.; Nikolov, S.G. Influence of the higher-order effects on the solutions of the complex cubic–quintic Ginzburg–Landau equation. *J. Mod. Opt.* **2020**, *67*, 606–618. [CrossRef]
63. Mihalache, D.; Mazilu, D.; Lederer, F.; Leblond, H.; Malomed, B.A. Collisions between coaxial vortex solitons in the three-dimensional cubic-quintic complex Ginzburg-Landau equation. *Phys. Rev. A* **2008**, *77*, 033817. [CrossRef]
64. Fang, J.J.; Mou, D.S.; Wang, Y.Y.; Zhang, H.C.; Dai, C.Q.; Chen, Y.X. Soliton dynamics based on exact solutions of conformable fractional discrete complex cubic Ginzburg–Landau equation. *Results Phys.* **2021**, *20*, 103710. [CrossRef]
65. Djoko, M.; Tabi, C.B.; Kofane, T.C. Effects of the septic nonlinearity and the initial value of the radius of orbital angular momentum beams on data transmission in optical fibers using the cubic-quintic-septic complex Ginzburg-Landau equation in presence of higher-order dispersions. *Chaos Solitons Fractals* **2021**, *147*, 110957. [CrossRef]
66. Mou, D.S.; Fang, J.J.; Fan, Y. Discrete localized excitations for discrete conformable fractional cubic–quintic Ginzburg–Landau model possessing the non-local quintic term. *Optik* **2021**, *244*, 167554. [CrossRef]
67. Liu, B.; Bo, W.; Liu, J.; Liu, J.; Shi, J.L.; Yuan, J.; Wu, Q. Simple harmonic and damped motions of dissipative solitons in two-dimensional complex Ginzburg-Landau equation supported by an external V-shaped potential. *Chaos Solitons Fractals* **2021**, *150*, 111126. [CrossRef]